RADIO-FREQUENCY RESONANCES OF A PARTIALLY IMMERSED WIRE IN MRI

PATRICE BOISSOLES, MARTIN COSTABEL, AND MONIQUE DAUGE

ABSTRACT. We study several mathematical and numerical models of resonance phenomena arising in Magnetic Resonance Imaging. We begin by describing eigenvalues and eigenfunctions of the Maxwell system with constant coefficients in a three-dimensional cylindrical domain. As particular cases, we find eigenpairs in a circular cylinder and in a circular cylinder with a coaxial circular hole. The corresponding eigenfrequencies give useful approximations of the resonance frequencies of a system consisting of a conducting wire embedded in homogeneous or heterogeneous physiological tissues encountered in MRI. We discretize this system with higher order finite elements and present computations describing the variations of the eigenfrequencies and of the structure of the eigenfunctions with respect to several relevant geometric and physical parameters.

CONTENTS

Date: September 21, 2006. Version 2.0.
1991 *Mathematics Subject Classification.* 78M10.
Key words and phrases. Keywords.

INTRODUCTION

S0

In this paper, we investigate the possible amplification in the presence of a conducting body of the electromagnetic field generated by an incident time-harmonic magnetic field.

The application which motivates our work comes from Magnetic Resonance Imaging (MRI): Under certain combinations of circumstances (frequency and geometry of the emitted magnetic field, nature and length of a conductor wire, position with respect to physiological tissues) it may happen that an important temperature increase at the surface of the conductor is observed. In real-life clinical situations, physiological effects have been observed that can go as far as severe tissue burning near the tip of the wire [12, 9].

From theoretical and experimental studies in the past decade, it has become clear [13, 19] that dangerous levels of local electromagnetic field concentration are not due to simple induction phenomena, but that they are caused by a *resonance* effect: Very strong local amplification of the field can occur at certain combinations of parameters, even if the conducting wire is placed at positions where the incident radio-frequency magnetic field has rather low amplitude. This happens if the (real) frequency of the incident field is close to the complex (in general non-real) eigenfrequency of the combined system of tissue and wire.

Studies of these local heating effects that have been conducted in order to establish general safety guidelines for MRI in the presence of conductors (pacemakers and other implants, guidewires for MRI-guided surgery, catheters or lengths of wire attached to measuring devices present during MRI scans) [15, 14, 20] have been based on extremely simplified models: circular loops or straight wires embedded in a homogeneous material. For more realistic models with heterogeneous environments, no general theoretical or experimental studies of the behavior of such resonance phenomena are available, and precise numerical models have only recently been considered [3].

Very recently, higher order finite element methods for the computation of Maxwell eigenvalue problems have been studied by several authors, but the geometry so far has been restricted to empty cavities [5, 11, 18].

In the present paper, we also consider simple model situations with a straight wire, but we study in particular the influence of a *heterogeneous* environment consisting of two different materials. This corresponds to the situation of a wire partially immersed in a weakly conducting liquid. In addition, whereas the computational domain is supposed to be axisymmetric, we consider the true magnetic field produced by a wire-frame antenna ("bird-cage" coil, *cf* Figure 1) as used in MRI [3, 4], acting on a wire parallel to, but not incident with, the axis of the bird-cage.

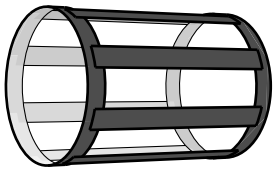

FIGURE 1. 3D view of a bird-cage coil with 8 legs figbirdcage

By using a high-precision numerical method (higher order finite elements, [17]), we study the dependency of the first few resonance frequencies and of the details of the corresponding amplified electromagnetic fields, on several relevant parameters: relative length and thickness of the wire, depth of the immersion, tissue conductivity, and artificial boundary conditions.

We combine the numerical model with a more simplified theoretical model and compare both, showing a good qualitative and quantitative agreement in many cases. The paper consists therefore of the following:

(1) The consideration of simplified model problems which have a cylindrical (cartesian product) geometry together with the assumption that the wire is a perfect conductor allow explicit analytic determination of the (real) eigenfrequencies.
(2) A larger class of model problems with axisymmetry geometry, consisting of a straight wire of finite conductivity embedded in a heterogeneous material and driven by the radio-frequency magnetic field of a small bird-cage antenna, can be numerically studied using a two-dimensional finite element discretization.
(3) The comparison of the two approaches results in an interesting agreement between a simple approximation by separation of variables and computations in a more realistic framework, as soon as appropriate boundary conditions are imposed. Ultimately, in the configuration of our numerical models, we obtain a 1D ("dipole antenna") approximation of the resonance effect within a 10% error bound.

More details of the organization of our paper are described at the end of the next section after the presentation of the mathematical model.

S1

1. THE MATHEMATICAL MODEL AND THE MODEL PROBLEMS

Let Ω be a bounded domain in $\mathbb{R}^3$ where the magnetic field $\mathbf{H}$ will be investigated. Let $\boldsymbol{\mathcal{H}}_{\mathsf{inc}}$ be the incident magnetic field. In our application $\boldsymbol{\mathcal{H}}_{\mathsf{inc}}$ is produced by a bird-cage antenna as specified in §4.1. For the numerical computations, we use the formulas established in [3, 4] for this field. It has the form of a time-harmonic field with angular frequency ω

$$\boldsymbol{\mathcal{H}}_{\mathsf{inc}}(x,t) = \mathrm{Re}\left(\exp(-i\omega t)\,\mathbf{H}_{\mathsf{inc}}(x)\right).$$

The range for ω is from 10^8 to $3\cdot 10^{10}$, corresponding to a frequency range between 15 MHz and 5 GHz. The incident field satisfies

1E0

$$\mathrm{div}\,\mathbf{H}_{\mathsf{inc}} = 0 \quad \text{in} \quad \Omega. \tag{1.1}$$

Let $\boldsymbol{\mathcal{H}}(x,t) = \mathrm{Re}\left(\exp(-i\omega t)\,\mathbf{H}(x)\right)$ be the scattered magnetic field: After a standard elimination of the electric field from Maxwell's equations, we find that $\mathbf{H}$ satisfies

1E1

$$\mathbf{curl}\left(\frac{1}{i\varepsilon\omega-\sigma}\,\mathbf{curl}\,\mathbf{H}\right) + i\omega\mu\mathbf{H} = -i\omega\mu\mathbf{H}_{\mathsf{inc}} \quad \text{in} \quad \Omega. \tag{1.2}$$

Here $\varepsilon = \varepsilon(x)$ and $\mu = \mu(x)$ are the electric permittivity and the magnetic permeability of the material(s) inside Ω, and $\sigma = \sigma(x)$ is the conductivity. In the whole paper we consider that, in standard SI units:

$$\mu \equiv \mu_0 = 4\pi\,10^{-7} \quad \text{in} \quad \Omega.$$

We will consider three different classes of configurations

A. The simple cavity filled with air: $\varepsilon \equiv \varepsilon_0 \simeq (36\pi)^{-1}10^{-9}$ in Ω and $\sigma \equiv 0$.

B. The situation of a metallic conductor body $\Omega_{\mathsf{cd}} \subset \Omega$ surrounded by air: $\varepsilon \equiv \varepsilon_0$ in Ω, and

$$\sigma = \sigma_0 \quad \text{in} \quad \Omega_{\mathsf{cd}} \quad \text{and} \quad \sigma = 0 \quad \text{in} \quad \Omega_{\mathsf{air}} := \Omega \setminus \Omega_{\mathsf{cd}}.$$

In most of the numerical experiments, σ_0 is taken to be 10^4.

C. The region around the metallic conductor is made of two sub-regions, one, Ω_{air}, filled with air as above, and the other, Ω_{swa}, with salted water (modelizing physiological tissues):

$$\Omega = \Omega_{\mathsf{cd}} \cup \Omega_{\mathsf{swa}} \cup \Omega_{\mathsf{air}}$$

and, in Ω_{swa}, $\varepsilon \equiv 80\,\varepsilon_0$ and $\sigma \equiv 4$, which correspond to a moderately conducting material.

Since $\omega \neq 0$, equations (1.1) and (1.2) imply that

1E2 (1.3) $$\operatorname{div} \mathbf{H} = 0 \quad \text{in} \quad \Omega.$$

The boundary conditions which have to be imposed to complement the equation (1.2) are artificial and thus, subject to discussion: A priori, they can be chosen among three types, with the outer unit normal field $\mathbf{n}$ to Ω:

(1) Perfect conductor boundary conditions: $\mathbf{H} \cdot \mathbf{n} = 0$,
(2) Perfect insulator boundary conditions: $\mathbf{H} \times \mathbf{n} = 0$,
(3) Impedance boundary conditions: $\mathbf{n} \times \mathbf{curl}\, \mathbf{H} + i\omega\varepsilon Z\, \mathbf{n} \times (\mathbf{n} \times \mathbf{H}) = 0$ with the impedance factor given by $Z = \left(\mu/(\varepsilon + \frac{i\sigma}{\omega})\right)^{1/2}$.

Note that the perfect insulator b.c. is the limit of the impedance b.c. as $Z \to \infty$, whereas the perfect conductor b.c. would be the limit of the impedance b.c. as $Z \to 0$.

Moreover, different boundary conditions can be imposed on different parts of $\partial\Omega$.

The *computational domain* Ω itself is, in a certain sense, artificial. From now on, we assume that it has the form of a cartesian product or cylinder (not necessarily of circular base)

1E4 (1.4) $$\Omega = G \times (a, b), \quad G \subset \mathbb{R}^2, \quad a < b.$$

Then, its boundary can be split into three parts:

$$\partial\Omega = G \times \{a\} \ \cup \ \partial G \times (a, b) \ \cup \ G \times \{b\}.$$

We will mainly consider the following combinations of boundary conditions

1E5 (1.5) $$\begin{cases} \mathbf{H} \cdot \mathbf{n} = 0 & & & \text{on} \quad \partial G \times (a, b) \\ \mathbf{H} \cdot \mathbf{n} = 0 & \text{or} & \mathbf{H} \times \mathbf{n} = 0 & \text{on} \quad G \times \{a\} \\ \mathbf{H} \cdot \mathbf{n} = 0 & \text{or} & \mathbf{H} \times \mathbf{n} = 0 & \text{on} \quad G \times \{b\}. \end{cases}$$

Note that, except in configuration **A.**, conditions (1.4)-(1.5) are not sufficient for problem (1.2) to have a tensor product structure that allows the use of separation of variables: In configuration **B.** for instance, we have a tensor product form if, moreover,

1E6 (1.6) $$\Omega_{\mathsf{cd}} = G_{\mathsf{cd}} \times (a,b), \quad G_{\mathsf{cd}} \subset G.$$

1D1 **Definition 1.1.** *Let V be the space of $L^2(\Omega)^3$ fields $\mathbf{H}$ satisfying $\mathbf{curl}\,\mathbf{H} \in L^2(\Omega)^3$, $\operatorname{div}\mathbf{H} \in L^2(\Omega)$ and the boundary conditions* (1.5)*. Let s be a positive parameter. The regularized variational formulation of our problem is:*

1E7 (1.7) *Find* $\mathbf{H} \in V$, *such that* $\forall \mathbf{H}' \in V$,

$$\int_\Omega \frac{1}{i\varepsilon\omega - \sigma}\,\mathbf{curl}\,\mathbf{H}\cdot\mathbf{curl}\,\bar{\mathbf{H}}'\,\mathrm{d}x - \int_\Omega is\,\operatorname{div}(\mu\mathbf{H})\operatorname{div}(\mu\bar{\mathbf{H}}')\,\mathrm{d}x + i\mu\omega\int_\Omega \mathbf{H}\cdot\bar{\mathbf{H}}'\,\mathrm{d}x = -i\mu\omega\int_\Omega \mathbf{H}_{\mathsf{inc}}\cdot\bar{\mathbf{H}}'\,\mathrm{d}x\,.$$

The regularization parameter s has no influence on the solution, since it will be chosen large enough to avoid spurious modes [10, 6, 7].

1.1. **Amplification of response.** For any fixed configuration in classes **A.**, **B.**, or **C.**, we vary ω and observe the behavior of the function

$$\omega \longmapsto \|\mathbf{H}(\omega)\|_{L^2(\Omega)^3}$$

with $\mathbf{H}(\omega)$ the solution of problem (1.7) for this ω. Our problem is to find and characterize the values of ω for which an amplification of the norm of $\mathbf{H}(\omega)$ occurs (resonances): The issue is to know whether, in the physical application, the presence of conducting parts leads to the appearance of small resonance values for ω.

In the medical literature, the frequency is usually kept fixed and the length of the wire is varied instead. This allows simpler experimental dispositions. In our case, the emphasis is on the precision of the numerical method, so we want to keep the computational domain and the mesh fixed for a series of parameter variations that display the resonance effects. The conclusions from both points of view should be equivalent, of course.

In problems of class **A.** ($\sigma \equiv 0$ in Ω), a (theoretically infinite) amplification occurs if and only if there exists an eigenpair $(\omega_0, \mathbf{H}_0)$ of the self-adjoint problem

1E8 (1.8) *Find* $\mathbf{H}_0 \in V$, $\mathbf{H}_0 \neq 0$, *and* $\omega_0 \in \mathbb{R}, \omega_0 > 0$ *such that* $\forall \mathbf{H}' \in V$,

$$\int_\Omega \mathbf{curl}\,\mathbf{H}_0\cdot\mathbf{curl}\,\bar{\mathbf{H}}'\,\mathrm{d}x = \varepsilon\mu\,\omega_0^2\int_\Omega \mathbf{H}_0\cdot\bar{\mathbf{H}}'\,\mathrm{d}x\,,$$

so that

1E9 (1.9) $$\omega \longrightarrow \omega_0 \quad \text{and} \quad \int_\Omega \mathbf{H}_{\mathsf{inc}}\cdot\bar{\mathbf{H}}_0\,\mathrm{d}x \neq 0.$$

Note that if (1.9) holds, problem (1.7) cannot be solved for $\omega = \omega_0$.

In configurations **B.** or **C.**, problem (1.7) is solvable for any real ω. An amplification occurs if there exists an eigenpair (ω_0, H_0) of the adjoint problem

1E10 (1.10) *Find* $\mathsf{H}_0 \in V$, $\mathsf{H}_0 \neq 0$, *and* $\omega_0 \in \mathbb{C}, \omega_0 \neq 0$ *such that* $\forall \mathsf{H}' \in V$,

$$\int_\Omega \frac{1}{i\varepsilon\omega_0 + \sigma} \mathbf{curl}\, \mathsf{H}_0 \cdot \mathbf{curl}\, \bar{\mathsf{H}}' \, \mathrm{d}x + i\mu\omega_0 \int_\Omega \mathsf{H}_0 \cdot \bar{\mathsf{H}}' \, \mathrm{d}x = 0$$

where ω_0 has a small imaginary part and

1E11 (1.11) $$\omega \longrightarrow \mathrm{Re}\, \omega_0 \quad \text{and} \quad \int_\Omega \mathsf{H}_{\mathsf{inc}} \cdot \bar{\mathsf{H}}_0 \, \mathrm{d}x \neq 0.$$

1.2. **Simplified configurations allowing the analytic determination of the spectrum.** In order to prove analytic formulas for the spectrum of problem (1.8), we will simply assume that we are in situation **A.** with Ω of cartesian product form (1.4).

The important point is the following: By the perfect conductor approximation, a configuration of type **B.** is transformed into a configuration of type **A.**, with the new domain $\Omega(\mathbf{A}) = \Omega(\mathbf{B}) \setminus \Omega_{\mathsf{cd}}$. The latter domain is of cartesian product form if and only if the conducting part satisfies (1.6), that is, the conductor part Ω_{cd} has the same length as Ω.

1.3. **More general configurations and FEM computations.** For the applications, the configurations of interest are of class **B.** or **C.**. A not a priori obvious question is whether the analysis of configurations **A.** can provide a relevant approximation for configurations of class **B.** or even **C.**, where the conductor Ω_{cd} is strictly contained in Ω, i.e., of the form

1E12 (1.12) $$\Omega_{\mathsf{cd}} = G_{\mathsf{cd}} \times (a_0, b_0), \quad \text{with} \quad G_{\mathsf{cd}} \subset G \quad \text{and} \quad a < a_0 < b_0 < b.$$

To answer this question, we perform computations based on a finite element discretization in axisymmetric configurations.

1.4. **Plan of the paper.** In §2 we give a full description of the Maxwell eigenpairs $\omega, (\mathsf{E}, \mathsf{H})$ in cylindrical domains Ω of class **A.** in terms of three families of modes: TE modes for which the electric part E, and not the magnetic part H, is transverse (the longitudinal component is 0), TM modes for which H (and not E) is transverse, and TEM modes for which both E and H are transverse. TEM modes have a 1D structure (i.e. their eigenvalues and eigenfunctions are completely described by those of a one-dimensional boundary value problem), they exist only if Ω is not simply connected, and they often contribute the lowest eigenvalues. In §3 we discuss this question in more details, with a special emphasis on axisymmetric domains for which fully analytic formulas can be provided using zeros of Bessel functions.

In §4 we specify the numerical model: We describe the incident field produced by the bird-cage antenna, and give details about the treatment of the metallic part, and about

the finite element code. In §5, we provide computations in situations **B.** very close to configurations of class **A.**, where the domain $\Omega = \Omega(\mathbf{B})$ contains a conductor part with high conductivity and same length as Ω. As a result, we obtain a very good agreement between computational and theoretical results for $\Omega(\mathbf{B})$ and $\Omega(\mathbf{A})$, respectively, linked by the relation $\Omega(\mathbf{A}) = \Omega(\mathbf{B}) \setminus \Omega_{\mathsf{cd}}$. In §6 we present computations for more realistic configurations **B.**, for which the conductor part is strictly shorter than the length of the computational domain. As a matter of fact, configurations **B.** for which the radius r_0 of Ω_{cd} tends to 0 while its conductivity σ tends to infinity keeping the ratio $r_0\sqrt{\sigma}$ constant, converge to a limiting configuration of class **A.**. In §7 we consider configurations **C.** where a part Ω_{swa} of the domain consists of a moderately conducting material. In all considered configurations **C.** we exhibit a correspondence between the lowest resonances and those of simplified configurations of class **A.** with appropriate boundary conditions. We conclude in §8.

S2

2. The Maxwell spectrum in cylindrical domains

Let $\Omega \subset \mathbb{R}^3$ be a cylinder, i.e. the cartesian product of a two-dimensional domain and an interval:

2E2

$$\Omega = G \times I, \quad G \subset \mathbb{R}^2, \ \ I = (a, b) \text{ interval in } \mathbb{R}. \tag{2.1}$$

We assume that G is a bounded Lipschitz domain. We note that the boundary of Ω is connected. But, if G is not simply connected, the same holds for Ω.

After defining notations for components and operators adapted to the cylindrical structure, we study the spectrum of the Maxwell operator with perfectly conducting, insulating and mixed boundary conditions in Ω. We introduce transverse electric and magnetic modes, exhibit explicit families of such eigenmodes of the Maxwell system as functions of scalar Dirichlet and Neumann problems on G and I. Finally we prove that these families are complete, thus generate the whole Maxwell spectrum.

2.1. Components and operators.

We denote Cartesian coordinates by

$$x = (x_1, x_2, x_3) = (x_\perp, x_3).$$

and, correspondingly, components by

$$\mathbf{u} = (u_1, u_2, u_3) = (\mathbf{u}_\perp, u_3).$$

Likewise, the exterior unit normal $\mathbf{n}$ to $\partial\Omega$ is written $(\mathbf{n}_\perp, n_3)$. On $G \times \partial I$, $\mathbf{n}_\perp = 0$ and $n_3 = \pm 1$. On $\partial G \times I$, $\mathbf{n}_\perp$ is the exterior unit normal to ∂G, $n_3 = 0$, and the tangential component of $\mathbf{u}_\perp$ is $\mathbf{u}_\perp \times \mathbf{n}_\perp = u_1 n_2 - u_2 n_1$.

The gradient and the Laplacian in the transverse plane are denoted by $\mathbf{grad}_\perp$ and $\Delta_\perp$:

$$\mathbf{grad}_\perp v = \begin{pmatrix} \partial_1 v \\ \partial_2 v \end{pmatrix} \quad \text{and} \quad \Delta_\perp v = \partial_1^2 v + \partial_2^2 v.$$

The vector and scalar curls in 2D are given by:

$$\mathbf{curl}_\perp\, v = \begin{pmatrix} \partial_2 v \\ -\partial_1 v \end{pmatrix} \quad \text{and} \quad \operatorname{curl}_\perp \mathbf{v} = \partial_1 v_2 - \partial_2 v_1.$$

We have the formula

2E3 (2.2) $$\mathbf{curl}\,\mathbf{u} = \begin{pmatrix} \partial_2 u_3 - \partial_3 u_2 \\ \partial_3 u_1 - \partial_1 u_3 \\ \partial_1 u_2 - \partial_2 u_1 \end{pmatrix} = \begin{pmatrix} \mathbf{curl}_\perp\, u_3 \\ \operatorname{curl}_\perp \mathbf{u}_\perp \end{pmatrix} + \partial_3 \begin{pmatrix} -u_2 \\ u_1 \\ 0 \end{pmatrix}.$$

The normal and tangential boundary conditions $\mathbf{u}\cdot\mathbf{n} = 0$ and $\mathbf{u}\times\mathbf{n} = 0$ on $\partial\Omega$ become, respectively

2E4a (2.3a) $$\begin{aligned} &\mathbf{u}_\perp \cdot \mathbf{n}_\perp = 0 \quad \text{on} \quad \partial G \times I, \\ &u_3 = 0 \quad \text{on} \quad G \times \partial I, \end{aligned}$$

and

2E4b (2.3b) $$\begin{aligned} &\mathbf{u}_\perp \times \mathbf{n}_\perp = 0 \quad \text{and} \quad u_3 = 0 \quad \text{on} \quad \partial G \times I, \\ &\mathbf{u}_\perp = 0 \quad \text{on} \quad G \times \partial I. \end{aligned}$$

2.2. **Definition of transverse modes.** After the standard rescaling $\sqrt{\varepsilon_0}\,\mathbf{E} \mapsto \mathbf{E}$ and $\sqrt{\mu_0}\,\mathbf{H} \mapsto \mathbf{H}$ and the introduction of the wave number $\kappa = \omega\sqrt{\varepsilon_0\mu_0}$, the Maxwell eigenmode problem can be written as

0E2

0E2a (2.4a) $$\begin{cases} \mathbf{curl}\,\mathbf{E} - i\kappa\mathbf{H} = 0 & \text{in} \quad \Omega, \\ \mathbf{curl}\,\mathbf{H} + i\kappa\mathbf{E} = 0 & \text{in} \quad \Omega, \\ \operatorname{div}\mathbf{E} = 0 \quad \text{and} \quad \operatorname{div}\mathbf{H} = 0 & \text{in} \quad \Omega. \end{cases}$$

with perfectly conducting boundary conditions

0E2b (2.4b) $$\mathbf{E}\times\mathbf{n} = 0 \quad \text{and} \quad \mathbf{H}\cdot\mathbf{n} = 0 \quad \text{on} \quad \partial\Omega.$$

We start the investigation of the solutions of (2.4) in a cylindrical domain by introducing special separation of variables Ansätze for the eigenmodes:

2D1 **Definition 2.1.** (i) *a TE* (Transverse Electric) *mode is a solution* $(\mathbf{E},\mathbf{H})$ *of* (2.4) *of the form*

TE (2.5) $$\mathbf{E}(x) = \begin{pmatrix} \mathbf{curl}_\perp\, v(x_\perp) \\ 0 \end{pmatrix} w(x_3) \quad \textit{and} \quad \mathbf{H} = \frac{1}{i\kappa}\,\mathbf{curl}\,\mathbf{E}$$

with scalar functions $v \in H^1(\Delta_\perp; G) := \{u \in H^1(G);\ \Delta_\perp u \in L^2(G)\}$, *and* $w \in H^1(I)$.

(ii) *a TM* (Transverse Magnetic) *mode is a solution* $(\mathbf{E},\mathbf{H})$ *of* (2.4) *of the form*

TM (2.6) $$\mathbf{H}(x)=\begin{pmatrix}\mathbf{curl}_\perp\, v(x_\perp)\\ 0\end{pmatrix} w(x_3) \quad \textit{and} \quad \mathbf{E}=-\frac{1}{i\kappa}\,\mathbf{curl}\,\mathbf{H}$$

with scalar functions $v\in H^1(\Delta_\perp;G)$ *and* $w\in H^1(I)$.

(iii) *a TEM mode is a solution* $(\mathbf{E},\mathbf{H})$ *of* (2.4) *of the form*

TEM (2.7) $$\mathbf{H}(x)=\begin{pmatrix}\mathbf{v}_\perp(x_\perp)\\ 0\end{pmatrix} w(x_3) \quad \textit{and} \quad \mathbf{E}(x)=\begin{pmatrix}\mathbf{v}'_\perp(x_\perp)\\ 0\end{pmatrix} w'(x_3)$$

with vector functions $\mathbf{v}_\perp$, $\mathbf{v}'_\perp$ *in* $L^2(G)^2$ *such that* $\mathrm{curl}_\perp\,\mathbf{v}_\perp$, $\mathrm{curl}_\perp\,\mathbf{v}'_\perp$, $\mathrm{div}_\perp\,\mathbf{v}_\perp$, $\mathrm{div}_\perp\,\mathbf{v}'_\perp$ *are all in* $L^2(G)$, *and scalar functions* w, $w'\in H^1(I)$.

2R1 *Remark* 2.2. For a field $\mathbf{u}$ of the form

T (2.8) $$\mathbf{u}(x)=\begin{pmatrix}\mathbf{curl}_\perp\, v(x_\perp)\\ 0\end{pmatrix} w(x_3),$$

the field $\mathbf{curl}\,\mathbf{u}$ is

Trot (2.9) $$\mathbf{curl}\,\mathbf{u}(x)=\begin{pmatrix}\mathbf{grad}_\perp\, v(x_\perp)\\ 0\end{pmatrix}\partial_3 w(x_3)-\begin{pmatrix}0\\ \Delta_\perp v(x_\perp)\end{pmatrix} w(x_3).$$

2.3. **TE modes.** Let $(\mathbf{E},\mathbf{H})$ be a couple of the form (2.5). We will exhibit sufficient conditions for $(\mathbf{E},\mathbf{H})$ to be a TE mode, and an explicit family of such modes. We find that $\mathrm{div}\,\mathbf{E}=0$ and that equations (2.4) reduce to

0E3 (2.10) $$\begin{cases}\mathbf{curl}\,\mathbf{curl}\,\mathbf{E}=\kappa^2\mathbf{E} & \text{in} \quad \Omega,\\ \mathbf{E}\times\mathbf{n}=0 & \text{on} \quad \partial\Omega.\end{cases}$$

Using formula (2.9) we obtain:

$$\mathbf{curl}\,\mathbf{curl}\,\mathbf{E}=-\begin{pmatrix}\mathbf{curl}_\perp\,\Delta_\perp v(x_\perp)\\ 0\end{pmatrix} w(x_3)-\begin{pmatrix}\mathbf{curl}_\perp\, v(x_\perp)\\ 0\end{pmatrix}\partial_3^2 w(x_3).$$

Thus we find that equation $\mathbf{curl}\,\mathbf{curl}\,\mathbf{E}=\kappa^2\mathbf{E}$ becomes

2E11 (2.11) $$-\begin{pmatrix}\mathbf{curl}_\perp\,\Delta_\perp v\\ 0\end{pmatrix} w-\begin{pmatrix}\mathbf{curl}_\perp\, v\\ 0\end{pmatrix}\partial_3^2 w \;=\; \kappa^2\begin{pmatrix}\mathbf{curl}_\perp\, v\\ 0\end{pmatrix} w.$$

Then we find that (2.11) holds if v and w satisfy

2E12 (2.12) $$-\Delta_\perp v=\lambda v \;\text{ in }\; G \quad\text{and}\quad -\partial_3^2 w=\mu w \;\text{ in }\; I \quad\text{with}\quad \lambda+\mu=\kappa^2.$$

Perfectly conducting boundary conditions on $\mathsf{E} \times \mathsf{n} = 0$ are satisfied if, cf (2.3b),

2E13 (2.13) $$\partial_n v = 0 \text{ on } \partial G \quad \text{and} \quad w = 0 \text{ on } \partial I.$$

The condition $\mathsf{E} \times \mathsf{n} = 0$ implies the condition $\mathsf{H} \cdot \mathsf{n} = 0$. Thus we have found the following families of TE modes:

2P1 **Proposition 2.3.** *Let*

$$\left(\lambda_j^{\mathsf{neu}}, v_j^{\mathsf{neu}}\right)_{j\geq 0} \quad \textit{with} \quad \lambda_0^{\mathsf{neu}} = 0 \quad \textit{and} \quad v_0^{\mathsf{neu}} = 1$$

be an orthonormal Neumann eigenpair sequence of the operator $-\Delta_\perp$ in G. Let

$$\left(\mu_k^{\mathsf{dir}}, w_k^{\mathsf{dir}}\right)_{k\geq 1}$$

be an orthonormal Dirichlet eigenpair sequence of the operator $-\partial_3^2$ in I. Then, for all $j \geq 1$, $k \geq 1$, the field $(\mathsf{E}_{jk}^{\mathsf{TE}}, \mathsf{H}_{jk}^{\mathsf{TE}})$

$$\mathsf{E}_{jk}^{\mathsf{TE}}(x) = \begin{pmatrix} \mathbf{curl}_\perp\, v_j^{\mathsf{neu}}(x_\perp) \\ 0 \end{pmatrix} w_k^{\mathsf{dir}}(x_3) \quad \textit{and} \quad \mathsf{H}_{jk}^{\mathsf{TE}} = \frac{1}{i\kappa_{jk}^{\mathsf{TE}}}\, \mathbf{curl}\, \mathsf{E}_{jk}^{\mathsf{TE}}$$

is a TE mode for problem (2.4) *associated with the eigenfrequency* $\kappa_{jk}^{\mathsf{TE}} = \sqrt{\lambda_j^{\mathsf{neu}} + \mu_k^{\mathsf{dir}}}$.

2.4. **TM modes.** Let (E, H) be a couple of the form (2.6). The derivation is the same for H as above for E, except concerning boundary conditions were we find now thanks to (2.3a) that $\mathsf{H} \cdot \mathsf{n} = 0$ if

2E13a (2.14) $$v = 0 \text{ on } \partial G.$$

We have also to check the condition $\mathsf{E} \times \mathsf{n} = 0$ for $\mathsf{E} = -(i\kappa)^{-1}\, \mathbf{curl}\, \mathsf{H}$, because this condition is not a consequence of $\mathsf{H} \cdot \mathsf{n} = 0$. We have

ETM (2.15) $$\mathsf{E} = \frac{1}{i\kappa} \begin{pmatrix} 0 \\ \Delta_\perp v(x_\perp) \end{pmatrix} w(x_3) - \frac{1}{i\kappa} \begin{pmatrix} \mathbf{grad}_\perp\, v(x_\perp) \\ 0 \end{pmatrix} \partial_3 w(x_3).$$

Taking the equation $\Delta_\perp v = \lambda v$ into account, we find that $\mathsf{E} \times \mathsf{n} = 0$ if (2.14) is satisfied, together with

2E13b (2.16) $$\partial_n w = 0 \text{ on } \partial I.$$

Now we have found the following families of TM modes:

2P2 **Proposition 2.4.** *Let*

$$\left(\lambda_j^{\mathsf{dir}}, v_j^{\mathsf{dir}}\right)_{j\geq 1}$$

be an orthonormal Dirichlet eigenpair sequence of the operator $-\Delta_\perp$ in G. Let

$$\left(\mu_k^{\mathsf{neu}}, w_k^{\mathsf{neu}}\right)_{k\geq 0} \quad \textit{with} \quad \mu_0^{\mathsf{neu}} = 0 \quad \textit{and} \quad w_0^{\mathsf{neu}} = 1$$

be an orthonormal Neumann eigenpair sequence of the operator $-\partial_3^2$ in I. Then, for all $j \geq 1$ and all $k \geq 0$, the field $(\mathsf{E}_{jk}^{\mathsf{TM}}, \mathsf{H}_{jk}^{\mathsf{TM}})$ with

$$\mathsf{H}_{jk}^{\mathsf{TM}}(x) = \begin{pmatrix} \mathbf{curl}_\perp\, v_j^{\mathsf{dir}}(x_\perp) \\ 0 \end{pmatrix} w_k^{\mathsf{neu}}(x_3) \quad \textit{and} \quad \mathsf{E}_{jk}^{\mathsf{TM}} = -\frac{1}{i\kappa_{jk}^{\mathsf{TM}}}\, \mathbf{curl}\, \mathsf{H}_{jk}^{\mathsf{TM}}$$

is a TM mode for problem (2.4) *associated with the eigenfrequency $\kappa_{jk}^{\mathsf{TM}} = \sqrt{\lambda_j^{\mathsf{dir}} + \mu_k^{\mathsf{neu}}}$.*

2.5. **TEM modes.** Let (E, H) be a couple of the form (2.7). We deduce from the equations $\mathbf{curl}\, \mathsf{H} + i\kappa \mathsf{E} = 0$ and $\operatorname{div} \mathsf{H} = 0$ that

2E20 (2.17) $$\operatorname{curl}_\perp \mathsf{v}_\perp = 0 \quad \text{and} \quad \operatorname{div}_\perp \mathsf{v}_\perp = 0 \quad \text{in} \quad G.$$

Taking the boundary conditions $\mathsf{H} \cdot \mathsf{n} = 0$ into account, we find that $\mathsf{v}_\perp$ belongs to the space $K_T(G)$ of no-flux harmonic vector fields:

$$K_T(G) = \{\mathbf{u}_\perp \in L^2(G)^2 \ :\ \operatorname{curl}_\perp \mathbf{u}_\perp = 0,\ \operatorname{div}_\perp \mathbf{u}_\perp = 0, \quad \mathbf{u}_\perp \cdot \mathbf{n}_\perp = 0 \ \text{ on } \ \partial G\}.$$

We can deduce from [1, Proposition 3.18]:

2L1 **Lemma 2.5.** (i) *If ∂G is connected, then $K_T(G) = \{0\}$.*
(ii) *If ∂G has $L+1$ connected components ($L \geq 1$), $\dim K_T(G) = L$: Let $\partial_0 G, \dots, \partial_L G$ be the connected components of ∂G. Let v_l^{top}, $l = 1, \dots, L$ be the harmonic potentials such that $v_l^{\mathsf{top}} = \delta_{lm}$ on $\partial_m G$, $m = 0, \dots, L$. Then there holds*

2E21 (2.18) $$K_T(G) = \operatorname{span}\{\mathbf{curl}_\perp\, v_1^{\mathsf{top}}, \dots, \mathbf{curl}_\perp\, v_L^{\mathsf{top}}\}.$$

Thus for H we are back to the situation of TM modes. We find:

2P3 **Proposition 2.6.** *If ∂G has $L+1$ connected components with $L \geq 1$, let $\left(v_l^{\mathsf{top}}\right)_{l=1,\dots,L}$ be the harmonic potentials defined in Lemma* 2.5. *Let $\left(\mu_k^{\mathsf{neu}}, w_k^{\mathsf{neu}}\right)$ for $k \geq 0$ be an orthonormal Neumann eigenpair sequence of the operator $-\partial_3^2$ in I, like in Proposition* 2.4. *Then, for all $l = 1, \dots, L$ and all $k \geq 0$, the field $(\mathsf{E}_{lk}^{\mathsf{TEM}}, \mathsf{H}_{lk}^{\mathsf{TEM}})$ with*

$$\mathsf{H}_{lk}^{\mathsf{TEM}}(x) = \begin{pmatrix} \mathbf{curl}_\perp\, v_l^{\mathsf{top}}(x_\perp) \\ 0 \end{pmatrix} w_k^{\mathsf{neu}}(x_3)$$

and

$$\mathbf{E}_{lk}^{\mathsf{TEM}} = -\frac{1}{i\kappa_k^{\mathsf{TEM}}}\,\mathbf{curl}\,\mathbf{H}_{lk}^{\mathsf{TEM}} \;\; \textit{if}\;\; k \geq 1 \quad \textit{and} \quad \mathbf{E}_{lk}^{\mathsf{TEM}} = 0 \;\; \textit{if}\;\; k = 0$$

is a TEM mode for problem (2.4) *associated with the eigenfrequency* $\kappa_k^{\mathsf{TEM}} = \sqrt{\mu_k^{\mathsf{neu}}}$.

2R2 *Remark* 2.7. *(i)* For $k \geq 1$ and a suitable choice of the normal eigenvectors w_k^{neu} and w_k^{dir}, we have the formula

$$\mathbf{E}_{lk}^{\mathsf{TEM}} = -\frac{1}{i\kappa_k^{\mathsf{TEM}}}\begin{pmatrix}\mathbf{grad}_\perp\, v_l^{\mathsf{top}}(x_\perp)\\ 0\end{pmatrix}\partial_3 w_k^{\mathsf{neu}}(x_3) = i\begin{pmatrix}\mathbf{grad}_\perp\, v_l^{\mathsf{top}}(x_\perp)\\ 0\end{pmatrix} w_k^{\mathsf{dir}}(x_3).$$

(ii) Let $\Theta(G)$ be the space defined as follows, cf [1]: Let G° be $G \setminus \Sigma$, where $\Sigma = \cup_{l=1}^{L}\Sigma_l$ is a minimal set of cuts so that G° is simply connected. Then

$$\Theta(G) = \{\varphi \in H^1(G^\circ);\quad \big[\varphi\big]_{\Sigma_l} = \mathrm{const}(l),\;\; l = 1,\dots,L\}.$$

For $\varphi \in \Theta(G)$, its extended curl, denoted $\widetilde{\mathbf{curl}}_\perp\,\varphi$, is its curl in G°, considered as an element of $L^2(G)$. Then there exists potentials $\tilde v_l^{\mathsf{top}} \in \Theta(G)$, such that for any $l = 1,\dots,L$, there holds

2E23 (2.20) $$\widetilde{\mathbf{curl}}_\perp\,\tilde v_l^{\mathsf{top}} = \mathbf{grad}_\perp\, v_l^{\mathsf{top}}.$$

Therefore for all $k \geq 1$, there holds

$$\mathbf{E}_{lk}^{\mathsf{TEM}}(x) = i\begin{pmatrix}\widetilde{\mathbf{curl}}_\perp\,\tilde v_l^{\mathsf{top}}(x_\perp)\\ 0\end{pmatrix} w_k^{\mathsf{dir}}(x_3).$$

2.6. **Completeness.** With the definitions introduced in Propositions 2.3, 2.4, 2.6, and Remark 2.7 we prove the following result.

2T1 **Theorem 2.8.** (i) *If* ∂G *is connected, a complete set of eigenmodes of* (2.4) *is given by*

2E30 (2.21) $$\big(\kappa_{jk}^{\mathsf{TE}};\mathbf{E}_{jk}^{\mathsf{TE}},\mathbf{H}_{jk}^{\mathsf{TE}}\big)_{j\geq1,\,k\geq1} \quad \textit{and} \quad \big(\kappa_{jk}^{\mathsf{TM}};\mathbf{E}_{jk}^{\mathsf{TM}},\mathbf{H}_{jk}^{\mathsf{TM}}\big)_{j\geq1,\,k\geq0}.$$

Here, for TE the eigenfrequency is $\kappa_{jk}^{\mathsf{TE}} = \sqrt{\lambda_j^{\mathsf{neu}} + \mu_k^{\mathsf{dir}}}$ *for* $j \geq 1,\; k \geq 1$, *and*

TE1 (2.22) $$\mathbf{E}_{jk}^{\mathsf{TE}} = \begin{pmatrix}\mathbf{curl}_\perp\, v_j^{\mathsf{neu}}(x_\perp)\\ 0\end{pmatrix} w_k^{\mathsf{dir}}(x_3), \qquad \mathbf{H}_{jk}^{\mathsf{TE}} = \frac{1}{i\kappa_{jk}^{\mathsf{TE}}}\,\mathbf{curl}\,\mathbf{E}_{jk}^{\mathsf{TE}}.$$

For TM, the eigenfrequency is $\kappa_{jk}^{\mathsf{TM}} = \sqrt{\lambda_j^{\mathsf{dir}} + \mu_k^{\mathsf{neu}}}$ *for* $j \geq 1,\; k \geq 0$, *and*

TM1 (2.23) $$\mathbf{H}_{jk}^{\mathsf{TM}} = \begin{pmatrix}\mathbf{curl}_\perp\, v_j^{\mathsf{dir}}(x_\perp)\\ 0\end{pmatrix} w_k^{\mathsf{neu}}(x_3), \qquad \mathbf{E}_{jk}^{\mathsf{TM}} = -\frac{1}{i\kappa_{jk}^{\mathsf{TM}}}\,\mathbf{curl}\,\mathbf{H}_{jk}^{\mathsf{TM}}.$$

(ii) *If ∂G has $L+1$ connected components ($L \geq 1$) a complete set of eigenmodes of* (2.4) *is given by the union of the modes* (2.21) *and the TEM modes*

2E31 (2.24) $$\left(\kappa_k^{\mathsf{TEM}}; \mathbf{E}_{lk}^{\mathsf{TEM}}, \mathbf{H}_{lk}^{\mathsf{TEM}}\right)_{l=1,\dots,L,\, k\geq 0}.$$

For TEM, the eigenfrequency is $\kappa_k^{\mathsf{TEM}} = \sqrt{\mu_k^{\mathsf{neu}}}$ for $k \geq 0$, and

TEM1 (2.25) $$\mathbf{E}_{lk}^{\mathsf{TEM}} = i \begin{pmatrix} \widetilde{\mathbf{curl}}_\perp\, \tilde v_l^{\mathsf{top}}(x_\perp) \\ 0 \end{pmatrix} w_k^{\mathsf{dir}}(x_3), \quad \mathbf{H}_{lk}^{\mathsf{TEM}} = \begin{pmatrix} \mathbf{curl}_\perp\, v_l^{\mathsf{top}}(x_\perp) \\ 0 \end{pmatrix} w_k^{\mathsf{neu}}(x_3)$$

where we set by convention $w_0^{\mathsf{dir}} = 0$.

Proof. In order to show completeness of the given set of eigenmodes, we prove that a divergence-free electric field which satisfies the boundary conditions and is orthogonal to the electric components of all modes is identically zero. A symmetric argument can be given for the magnetic component.

Thus let $\mathbf{u} \in L^2(\Omega)^3$ such that $\mathbf{curl}\,\mathbf{u} \in L^2(\Omega)^3$, $\operatorname{div}\mathbf{u} = 0$ and $\mathbf{u}\times\mathbf{n} = 0$ on $\partial\Omega$. We assume that for all integers $j \geq 1$ and $l \in [1, L]$

$$\langle \mathbf{u}, \mathbf{E}_{jk}^{\mathsf{TE}}\rangle = 0 \ \ (\forall k \geq 1), \quad \langle \mathbf{u}, \mathbf{E}_{jk}^{\mathsf{TM}}\rangle = 0 \ \ (\forall k \geq 0) \quad \text{and} \quad \langle \mathbf{u}, \mathbf{E}_{lk}^{\mathsf{TEM}}\rangle = 0 \ \ (\forall k \geq 1).$$

Here $\langle\cdot,\cdot\rangle$ is the L^2 scalar product on Ω. We have to show $\mathbf{u} = 0$.

We first draw consequences from the orthogonality properties against the TM modes: We fix j and k, set $v = v_j^{\mathsf{dir}}$, $w = w_k^{\mathsf{neu}}$, use $\mathbf{E}^{\mathsf{TM}}$ in the form (2.15) and integrate by parts:

$$\begin{aligned}
0 &= \int_I\int_G \mathbf{u}_\perp(x_\perp,x_3)\ \mathbf{grad}_\perp\, v(x_\perp)\partial_3 w(x_3) - u_3(x_\perp,x_3)\,\Delta_\perp v(x_\perp) w(x_3)\ \mathrm{d}x_\perp\mathrm{d}x_3 \\
&= \int_I\int_G -\operatorname{div}_\perp \mathbf{u}_\perp(x_\perp,x_3)\, v(x_\perp)\partial_3 w(x_3) - u_3(x_\perp,x_3)\,\Delta_\perp v(x_\perp) w(x_3)\ \mathrm{d}x_\perp\mathrm{d}x_3 \\
&= \int_I\int_G \partial_3 u_3(x_\perp,x_3)\, v(x_\perp)\partial_3 w(x_3) - u_3(x_\perp,x_3)\,\Delta_\perp v(x_\perp) w(x_3)\ \mathrm{d}x_\perp\mathrm{d}x_3 \\
&= \int_I\int_G -u_3(x_\perp,x_3)\, v(x_\perp)\partial_3^2 w(x_3) - u_3(x_\perp,x_3)\,\Delta_\perp v(x_\perp) w(x_3)\ \mathrm{d}x_\perp\mathrm{d}x_3.
\end{aligned}$$

Here we have used that $\operatorname{div}\mathbf{u} = 0$, replacing $\operatorname{div}_\perp \mathbf{u}_\perp$ by $-\partial_3 u_3$. Coming back to the properties of $v = v_j^{\mathsf{dir}}$ and $w = w_k^{\mathsf{neu}}$ we find for all $j \geq 1$ and $k \geq 0$

$$\int_I\int_G u_3(x_\perp,x_3)\,(\lambda_j^{\mathsf{dir}} + \mu_k^{\mathsf{neu}}) v_j^{\mathsf{dir}}(x_\perp) w_k^{\mathsf{neu}}(x_3)\ \mathrm{d}x_\perp\mathrm{d}x_3 = 0.$$

Since $\lambda_j^{\mathsf{dir}} + \mu_k^{\mathsf{neu}}$ is never 0, we deduce that for all $j \geq 1$ and $k \geq 0$

$$\int_I\int_G u_3(x_\perp,x_3)\, v_j^{\mathsf{dir}}(x_\perp) w_k^{\mathsf{neu}}(x_3)\ \mathrm{d}x_\perp\mathrm{d}x_3 = 0.$$

The set $v_j^{\mathsf{dir}}(x_\perp)w_k^{\mathsf{neu}}(x_3)$ being a complete basis in $L^2(\Omega)$, we deduce that $u_3 = 0$.

Next, we use the orthogonality against the TE modes: for all $j \geq 1$ and $k \geq 1$ there holds:

$$\int_I w_k^{\mathsf{dir}}(x_3) \int_G \mathbf{u}_\perp(x_\perp, x_3) \cdot \mathbf{curl}_\perp\, v_j^{\mathsf{neu}}(x_\perp)\, \mathrm{d}x_\perp \mathrm{d}x_3 = 0.$$

Therefore, for all $j \geq 1$:

$$\int_G \mathbf{u}_\perp(x_\perp, x_3) \cdot \mathbf{curl}_\perp\, v_j^{\mathsf{neu}}(x_\perp)\, \mathrm{d}x_\perp = 0, \quad \forall x_3 \in I.$$

We deduce that $\mathrm{curl}_\perp\, \mathbf{u}_\perp(\cdot, x_3)$ is orthogonal to all v_j^{neu} for $j \geq 1$, which means that $\mathrm{curl}_\perp\, \mathbf{u}_\perp(\cdot, x_3)$ is constant with respect to $x_\perp$. There exists a function $z = z(x_3)$ such that

$$(*) \qquad \mathrm{curl}_\perp\, \mathbf{u}_\perp(x_\perp, x_3) = z(x_3).$$

Since $\mathrm{div}\, \mathbf{u} = 0$ and $u_3 = 0$, we have $\mathrm{div}_\perp\, \mathbf{u}_\perp = 0$. Besides, the orthogonality relations against the TEM modes yields for all $k \geq 1$ and $l \leq L$

$$\int_I w_k^{\mathsf{dir}}(x_3) \int_G \mathbf{u}_\perp(x_\perp, x_3) \cdot \mathbf{grad}_\perp\, v_l^{\mathsf{top}}(x_\perp)\, \mathrm{d}x_\perp \mathrm{d}x_3 = 0.$$

We deduce that

$$\int_G \mathbf{u}_\perp(x_\perp, x_3) \cdot \mathbf{grad}_\perp\, v_l^{\mathsf{top}}(x_\perp)\, \mathrm{d}x_\perp = 0, \quad \forall x_3 \in I,$$

from which we find that

$$\int_{\partial_l G} \mathbf{u}_\perp \cdot \mathbf{n}_\perp\, \mathrm{d}\sigma = 0, \quad l = 1, \ldots, L.$$

Combined with $\mathrm{div}_\perp\, \mathbf{u}_\perp = 0$, this provides the existence of a potential $y \in L^2(I, H^1(G))$ satisfying the Neumann boundary condition on ∂G such that

$$\mathbf{u}_\perp(x_\perp, x_3) = \mathbf{curl}_\perp\, y(x_\perp, x_3).$$

With $(*)$ we find

$$-\Delta_\perp y(x_\perp, x_3) = z(x_3).$$

Since y satisfies the homogeneous Neumann condition with respect to $x_\perp$, this implies that $z(x_3) = 0$ for all x_3. Finally we have obtained that $\mathbf{u}_\perp = 0$. □

2.7. **Mixed boundary conditions.** Our results can be adapted to describe the spectrum of the Maxwell problem (2.4a), with instead of boundary conditions (2.4b), the mixed boundary conditions

0E3a (2.26a)
$$\left\{\begin{array}{rcl} \mathbf{E}\times\mathbf{n} &=& 0 \quad \text{and} \quad \mathbf{H}\cdot\mathbf{n} = 0 \quad \text{on} \quad \partial G\times I,\\ \mathbf{E}\cdot\mathbf{n} &=& 0 \quad \text{and} \quad \mathbf{H}\times\mathbf{n} = 0 \quad \text{on} \quad G\times\{a\},\\ \mathbf{E}\cdot\mathbf{n} &=& 0 \quad \text{and} \quad \mathbf{H}\times\mathbf{n} = 0 \quad \text{on} \quad G\times\{b\}, \end{array}\right.$$

or

0E3b (2.26b)
$$\left\{\begin{array}{rcl} \mathbf{E}\times\mathbf{n} &=& 0 \quad \text{and} \quad \mathbf{H}\cdot\mathbf{n} = 0 \quad \text{on} \quad \partial G\times I,\\ \mathbf{E}\cdot\mathbf{n} &=& 0 \quad \text{and} \quad \mathbf{H}\times\mathbf{n} = 0 \quad \text{on} \quad G\times\{a\},\\ \mathbf{E}\times\mathbf{n} &=& 0 \quad \text{and} \quad \mathbf{H}\cdot\mathbf{n} = 0 \quad \text{on} \quad G\times\{b\}. \end{array}\right.$$

Adapting the proofs above, we find that the results of Propositions 2.3, 2.4 and 2.6 and of Theorem 2.8 can be extended to the situations of boundary conditions (2.26a) and (2.26b) according to:

2T2 **Theorem 2.9.** (i) *If ∂G is connected, a complete set of eigenmodes of the Maxwell equations* (2.4a) *with boundary conditions* (2.26a) *or* (2.26b) *is given by*

2E40 (2.27)
$$\big(\kappa^{\mathsf{TE}}_{jk};\mathbf{E}^{\mathsf{TE}}_{jk},\mathbf{H}^{\mathsf{TE}}_{jk}\big)_{j\geq1,\,k\geq0 \text{ or } 1} \quad \textit{and} \quad \big(\kappa^{\mathsf{TM}}_{jk};\mathbf{E}^{\mathsf{TM}}_{jk},\mathbf{H}^{\mathsf{TM}}_{jk}\big)_{j\geq1,\,k\geq0 \text{ or } 1}.$$

(a) *In case of boundary conditions* (2.26a)*:*
The TE eigenfrequency is $\kappa^{\mathsf{TE}}_{jk}=\sqrt{\lambda^{\mathsf{neu}}_j+\mu^{\mathsf{neu}}_k}$ for $j\geq1,\ k\geq0$, and

TE2 (2.28)
$$\mathbf{E}^{\mathsf{TE}}_{jk}=\begin{pmatrix}\mathbf{curl}_\perp\, v^{\mathsf{neu}}_j(x_\perp)\\ 0\end{pmatrix} w^{\mathsf{neu}}_k(x_3),\qquad \mathbf{H}^{\mathsf{TE}}_{jk}=\frac{1}{i\kappa^{\mathsf{TE}}_{jk}}\,\mathbf{curl}\,\mathbf{E}^{\mathsf{TE}}_{jk}.$$

The TM eigenfrequency is $\kappa^{\mathsf{TM}}_{jk}=\sqrt{\lambda^{\mathsf{dir}}_j+\mu^{\mathsf{dir}}_k}$ for $j\geq1,\ k\geq1$, and

TM2 (2.29)
$$\mathbf{H}^{\mathsf{TM}}_{jk}=\begin{pmatrix}\mathbf{curl}_\perp\, v^{\mathsf{dir}}_j(x_\perp)\\ 0\end{pmatrix} w^{\mathsf{dir}}_k(x_3),\qquad \mathbf{E}^{\mathsf{TM}}_{jk}=-\frac{1}{i\kappa^{\mathsf{TM}}_{jk}}\,\mathbf{curl}\,\mathbf{H}^{\mathsf{TM}}_{jk}$$

(b) *In case of boundary conditions* (2.26b)*:*
The TE eigenfrequency is $\kappa^{\mathsf{TE}}_{jk}=\sqrt{\lambda^{\mathsf{neu}}_j+\mu^{\mathsf{nd}}_k}$ for $j\geq1,\ k\geq1$, and

TE3 (2.30)
$$\mathbf{E}^{\mathsf{TE}}_{jk}=\begin{pmatrix}\mathbf{curl}_\perp\, v^{\mathsf{neu}}_j(x_\perp)\\ 0\end{pmatrix} w^{\mathsf{nd}}_k(x_3),\qquad \mathbf{H}^{\mathsf{TE}}_{jk}=\frac{1}{i\kappa^{\mathsf{TE}}_{jk}}\,\mathbf{curl}\,\mathbf{E}^{\mathsf{TE}}_{jk}$$

The TM eigenfrequency is $\kappa_{jk}^{\mathsf{TM}} = \sqrt{\lambda_j^{\mathsf{dir}} + \mu_k^{\mathsf{dn}}}$ *for* $j \geq 1,\ k \geq 1$, *and*

TM3 (2.31) $$\mathbf{H}_{jk}^{\mathsf{TM}} = \begin{pmatrix} \mathbf{curl}_\perp\, v_j^{\mathsf{dir}}(x_\perp) \\ 0 \end{pmatrix} w_k^{\mathsf{dn}}(x_3), \qquad \mathbf{E}_{jk}^{\mathsf{TM}} = -\frac{1}{i\kappa_{jk}^{\mathsf{TM}}}\, \mathbf{curl}\, \mathbf{H}_{jk}^{\mathsf{TM}}$$

Here $(\mu_k^{\mathsf{nd}}, w_k^{\mathsf{nd}})$ *and* $(\mu_k^{\mathsf{dn}}, w_k^{\mathsf{dn}})$ *for* $k \geq 1$ *is an orthonormal eigenpair sequence of the operator* $-\partial_3^2$ *in* I *with boundary conditons* $w'(a) = w(b) = 0$ *and* $w(a) = w'(b) = 0$, *respectively.*

(ii) *If* ∂G *has* $L+1$ *connected components* ($L \geq 1$) *a complete set of eigenmodes of* (2.4) *is given by the reunion of the above modes* (2.27) *and the TEM modes*

2E41 (2.32) $$\left(\kappa_k^{\mathsf{TEM}}; \mathbf{E}_{lk}^{\mathsf{TEM}}, \mathbf{H}_{lk}^{\mathsf{TEM}}\right)_{l=1,\dots,L,\, k\geq 0 \text{ or } 1}.$$

(a) *In case of boundary conditions* (2.26a), $\kappa_k^{\mathsf{TEM}} = \sqrt{\mu_k^{\mathsf{neu}}}$ *and*

TEM2 (2.33) $$\mathbf{E}_{lk}^{\mathsf{TEM}} = i \begin{pmatrix} \widetilde{\mathbf{curl}}_\perp\, \tilde{v}_l^{\mathsf{top}}(x_\perp) \\ 0 \end{pmatrix} w_k^{\mathsf{neu}}(x_3), \quad \mathbf{H}_{lk}^{\mathsf{TEM}} = \begin{pmatrix} \mathbf{curl}_\perp\, v_l^{\mathsf{top}}(x_\perp) \\ 0 \end{pmatrix} w_k^{\mathsf{dir}}(x_3)$$

for $k \geq 0$, *where by convention,* w_0^{dir} *is set to* 0.

(b) *In case of boundary conditions* (2.26b), $\kappa_k^{\mathsf{TEM}} = \sqrt{\mu_k^{\mathsf{nd}}} = \sqrt{\mu_k^{\mathsf{dn}}}$, $k \geq 1$, *and:*

TEM3 (2.34) $$\mathbf{E}_{lk}^{\mathsf{TEM}} = i \begin{pmatrix} \widetilde{\mathbf{curl}}_\perp\, \tilde{v}_l^{\mathsf{top}}(x_\perp) \\ 0 \end{pmatrix} w_k^{\mathsf{nd}}(x_3), \quad \mathbf{H}_{lk}^{\mathsf{TEM}} = \begin{pmatrix} \mathbf{curl}_\perp\, v_l^{\mathsf{top}}(x_\perp) \\ 0 \end{pmatrix} w_k^{\mathsf{dn}}(x_3).$$

S3 3. The smallest eigenfrequencies in cylindrical domains

3.1. **Influence of a conductor part.** We still consider the case when $\Omega = G \times I$. Let ℓ be the length of I. We assume that ∂G is connected (or, equivalently, that G is simply connected). Then the smallest eigenfrequency in the case of boundary conditions (2.4b) is positive and equal to

3E1 (3.1) $$\min\left\{ \sqrt{\lambda_1^{\mathsf{neu}}(G) + \frac{\pi^2}{\ell^2}},\ \sqrt{\lambda_1^{\mathsf{dir}}(G)} \right\}.$$

Let us now assume that Ω contains a conductor part $\Omega_{\mathsf{cd}} = G_{\mathsf{cd}} \times I$, with $\overline{G}_{\mathsf{cd}} \subset G$. If we use the perfect conductor approximation, we look for the eigenfrequencies in

3E2 (3.2) $$\Omega' = G' \times I, \quad G' = G \setminus G_{\mathsf{cd}}.$$

Then G' is not simply connected and the first non-zero TEM eigenfrequency of Ω' is $\frac{\pi}{\ell}$. Thus, as soon as

3E3 (3.3) $$\frac{\pi}{\ell} < \sqrt{\lambda_1^{\mathsf{dir}}(G)}\,,$$

the domain Ω' has a positive TEM eigenfrequency smaller than all eigenfrequencies of the domain Ω. In case of boundary conditions (2.26a), inequality (3.3) is replaced with $\frac{\pi}{\ell} < \sqrt{\lambda_1^{\mathsf{neu}}(G)}$. *In the case of the mixed boundary conditions* (2.26b) *the lowest TEM eigenfrequency of Ω' is always smaller than the eigenfrequencies of Ω.* We consider now the specific situation of axisymmetric cylindrical domains.

3.2. **Case of axisymmetric domains.** We assume that G is a disk of radius R, centered at O, and G_{cd} is a concentric disk of radius $r_0 < R$. Thus, G' is an annulus of internal radius r_0 and external radius R. Both domains Ω and Ω_{cd} are circular cylinders.

We use *cylindrical coordinates* $(r, \theta, z) \in (0, R) \times [0, 2\pi) \times I$. For a scalar function $u = u(x)$, let $\check{u}$ be its expression in cylindrical coordinates: $\check{u}(r, \theta, z) = u(x)$. Additionally, for a vector field $\mathbf{u} = (u_1, u_2, u_3)$, we introduce its *cylindrical components* (u_r, u_θ, u_z) according to

$$u_r = \check{u}_1 \cos\theta + \check{u}_2 \sin\theta, \quad u_\theta = -\check{u}_1 \sin\theta + \check{u}_2 \cos\theta \quad \text{and} \quad u_z = \check{u}_3.$$

The notion of angular Fourier modes makes sense (see [2] for more details):

5D1 **Definition 3.1.** *Let u be a scalar function in $L^2(\Omega)$ and let $\check{u}$ be the function defined on $(0, R) \times [0, 2\pi) \times I$ by $\check{u}(r, \theta, z) = u(x)$. For any $n \in \mathbb{Z}$, the angular Fourier coefficient of order n of u is denoted by u^n and is defined as:*

5E3 (3.4) $$u^n(r, z) = \frac{1}{\sqrt{2\pi}} \int_0^{2\pi} \check{u}(r, \theta, z)\, e^{-in\theta}\, \mathrm{d}\theta, \quad 0 < r < R, \ \ z \in I.$$

Let $\mathbf{u} = (u_1, u_2, u_3)$ be a vector field in $L^2(\Omega)^3$. For any $n \in \mathbb{Z}$, the angular Fourier coefficient of order n of $\mathbf{u}$, denoted bu $\mathbf{u}^n$, is defined as

5E3b (3.5) $$\mathbf{u}^n = (u_r^n, u_\theta^n, u_z^n).$$

For a scalar function v, the radial and angular components of $\mathbf{grad}_\perp\, v$ are $\partial_r v$ and $\frac{1}{r}\partial_\theta v$, and those of $\mathbf{curl}_\perp\, v$ are $\frac{1}{r}\partial_\theta v$ and $-\partial_r v$. Likewise, the cylindrical components of $\mathbf{curl}\,\mathbf{u}$ are

3Er (3.6) $$\begin{cases} (\mathbf{curl}\,\mathbf{u})_r = \frac{1}{r}\partial_\theta u_z - \partial_z u_\theta, \\ (\mathbf{curl}\,\mathbf{u})_\theta = \partial_z u_r - \partial_r u_z, \\ (\mathbf{curl}\,\mathbf{u})_z = \partial_r u_\theta + \frac{1}{r} u_\theta - \frac{1}{r}\partial_\theta u_r. \end{cases}$$

Since the coefficients in (3.6) do not depend on θ, the spectrum of the Maxwell operator (2.4) on the cylinders Ω or Ω' commutes with the self-adjoint operator $i\partial_\theta$. Therefore there exists a basis of eigenvectors of (2.4) such that each of its elements $(\mathbf{E}, \mathbf{H})$ satisfies

3E30 (3.7) $$\exists n \in \mathbb{Z} \quad \text{such that} \quad (\mathbf{E}^n, \mathbf{H}^n) \not\equiv 0 \quad \text{and} \quad \forall m \neq n, \quad \mathbf{E}^m = \mathbf{H}^m = 0.$$

The integer n is called the *order* of the eigenmode. For any $n \in \mathbb{Z}$ there exists a countably infinite family of orthogonal eigenvectors of order n.

Of course, this is compatible with the TE and TM structures. The Dirichlet and Neumann problems for $\Delta_\perp$ in G or G' are axisymmetric problems. Therefore, they also commute with $i\partial_\theta$ and share with $i\partial_\theta$ a common eigenvector basis. Hence the eigenvectors of the Dirichlet and Neumann problems in G or G' can be classified according to their angular Fourier coefficient like in (3.7): For each eigenvector v there exists an integer n such that

3E31 (3.8) $$v(x_\perp) = \frac{1}{\sqrt{2\pi}} v^n(r)\, e^{in\theta} \quad \text{in} \quad G \quad \text{or} \quad G',$$

3E32 and v^n is solution of the Bessel equation

3E32a (3.9a) $$-\left(r^2\partial_r^2 + r\partial_r - n^2\right) v^n = \lambda v^n \quad \text{in} \quad (0, R) \quad \text{or} \quad (r_0, R).$$

This provides a natural classification for the TE and TM modes in Ω and Ω': As a consequence of Theorems 2.8 and 2.9, we find

3C1 **Proposition 3.2.** *Let Ω by a circular cylinder of radius R and $\Omega' = \Omega \setminus \Omega_{\mathsf{cd}}$, with Ω_{cd} a coaxial cylinder of radius r_0 and the same length.*

(i) *Each TE mode in Ω or Ω' can be classified by its order n: It has the form* (2.22), (2.28) *or* (2.30) *for $v_j^{\mathsf{neu}} = v$ satisfying* (3.8) *with a (non-constant) eigenvector v^n of problem* (3.9a) *complemented by boundary conditions in* 0 *or* r_0

3E32b (3.9b) $$\begin{cases} v^n(0) = 0 & \text{if} \quad n \neq 0, \\ \partial_r v^n(0) = 0 & \text{if} \quad n = 0, \end{cases} \quad \text{for} \quad \Omega \quad \text{or} \quad \partial_r v^n(r_0) = 0 \quad \text{for} \quad \Omega'$$

and in R

3E32c (3.9c) $$\partial_r v^n(R) = 0.$$

(ii) *Likewise, the TM modes of order n are given by* (2.23), (2.29) *or* (2.31) *for $v_j^{\mathsf{dir}} = v$ satisfying* (3.8) *with an eigenvector v^n of* (3.9a) *with boundary conditions in* 0 *or* r_0

3E32d (3.9d) $$\begin{cases} v^n(0) = 0 & \text{if} \quad n \neq 0, \\ \partial_r v^n(0) = 0 & \text{if} \quad n = 0, \end{cases} \quad \text{for} \quad \Omega \quad \text{or} \quad v^n(r_0) = 0 \quad \text{for} \quad \Omega'$$

and in R

3E32e (3.9e) $$v^n(R) = 0.$$

In Ω' appear the TEM modes: $\partial G'$ has two connected components, and the generator v^{top} can be defined as the function $x \mapsto \log r$. It is axisymmetric (i.e. of order $n = 0$), therefore the TEM modes are axisymmetric, too. In connection with Remark 2.7, we note that the "conjugate" potential $\tilde{v}^{\mathsf{top}}$ is the function $x \mapsto \theta$. There holds, *cf* (2.17):

3E38 (3.10) $$\widetilde{\mathbf{curl}}_\perp\, \tilde{v}^{\mathsf{top}} = \mathbf{grad}_\perp\, v^{\mathsf{top}} = \begin{pmatrix} \frac{1}{r} \\ 0 \\ 0 \end{pmatrix} \quad \text{and} \quad \mathbf{curl}_\perp\, v^{\mathsf{top}} = -\begin{pmatrix} 0 \\ \frac{1}{r} \\ 0 \end{pmatrix}.$$

Hence we obtain for TEM modes:

3C2 **Proposition 3.3.** *Let* $\Omega' = \Omega \setminus \Omega_{\mathsf{cd}}$*, with* Ω *and* Ω_{cd} *coaxial cylinders of radii* R *and* r_0 *and the same length. The TEM modes in* Ω' *are axisymmetric (i.e. their cylindrical components do not depend on* θ*) and have the form*

5E15 (3.11) $$\begin{cases} E_r = \frac{i}{\kappa r}\, \partial_z w(z), \\ E_\theta = 0, \\ E_z = 0, \end{cases} \quad \textit{and} \quad \begin{cases} H_r = 0, \\ H_\theta = -\frac{1}{r}\, w(z), \\ H_z = 0. \end{cases}$$

3R1 *Remark* 3.4. As r_0 tends to 0, the Dirichlet and Neumann eigenmodes of the annulus tend to the Dirichlet and Neumann eigenvalues of the disk of same radius. Hence the TE and TM modes of the cylinder with hole Ω' tend to the TE and TM modes of the cylinder without hole Ω. In contrast, the TEM modes do not depend on r_0 as long as $r_0 \neq 0$, but disappear at the limit when $r_0 = 0$. This fact has a practical importance when thin conductor wires are present.

3.3. **Dirichlet and Neumann eigenvalues in a disk.** Let G be the disk of radius R. The Dirichlet and Neumann eigenvectors for $-\Delta_\perp$ in G have the form (3.8), with v^n scaled from the Bessel function of the first kind $J_n(z)$, solution of the differential equation

$$x^2 y'' + xy' + (x^2 - n^2)y = 0,$$

bounded in $x = 0$. Moreover, $J_0(0) = 1$ and $J_0'(0) = 0$, and $J_n(0) = \mathcal{O}(x^n)$.

6L1 **Lemma 3.5** ([8])**.** (i) *Let* $(z^{\mathsf{dir}}_{n,m})_{m\geq 1}$ *be the positive zeros of* J_n*. The eigenpairs of* (3.9a) *with boundary conditions* (3.9d) *in* $r = 0$ *and* (3.9e) *in* $r = R$ *are* $(\lambda^{\mathsf{dir}}_{n,m}, v^{\mathsf{dir}}_{n,m})$ *with*

6E1 (3.12) $$\lambda^{\mathsf{dir}}_{n,m} = \left(\frac{z^{\mathsf{dir}}_{n,m}}{R}\right)^2 \quad \textit{and} \quad v^{\mathsf{dir}}_{n,m}(r) = J_n\Big(z^{\mathsf{dir}}_{n,m}\frac{r}{R}\Big), \quad n \geq 0, \quad m \geq 1.$$

(ii) *Let* $(z^{\mathsf{neu}}_{n,m})_{m\geq 1}$ *be the positive zeros of* J'_n. *The eigenpairs of* (3.9a) *with boundary conditions* (3.9b) *in* $r=0$ *and* (3.9c) *in* $r=R$ *are* $(\lambda^{\mathsf{neu}}_{n,m}, v^{\mathsf{neu}}_{n,m})$ *with*

6E2 (3.13) $$\lambda^{\mathsf{neu}}_{n,m} = \left(\frac{z^{\mathsf{neu}}_{n,m}}{R}\right)^2 \quad \textit{and} \quad v^{\mathsf{neu}}_{n,m}(r) = J'_n\Big(z^{\mathsf{neu}}_{n,m}\frac{r}{R}\Big), \quad n\geq 0, \quad m\geq 1.$$

In Table 1 we give values for the first three zeros $z^{\mathsf{dir}}_{n,m}$ and $z^{\mathsf{neu}}_{n,m}$ for $n=0,1,2$. We use the relation $J_{\nu-1}-J_{\nu+1}=2J'_\nu$ to compute $z^{\mathsf{neu}}_{n,m}$. Since $J_{-1}=-J_1$, there holds

$$z^{\mathsf{neu}}_{0,m} = z^{\mathsf{dir}}_{1,m}, \quad \forall m\geq 1.$$

$z^{\mathsf{dir}}_{0,m}$	$z^{\mathsf{dir}}_{1,m}$	$z^{\mathsf{dir}}_{2,m}$	$z^{\mathsf{neu}}_{0,m}$	$z^{\mathsf{neu}}_{1,m}$	$z^{\mathsf{neu}}_{2,m}$
2.4048	3.8317	5.1356	3.8317	1.8412	3.0542
5.5201	7.0156	8.4172	7.0156	5.3314	6.7061
8.6537	10.173	11.620	10.173	8.5363	9.9695

t1s3 TABLE 1. The first three zeros of J_0, J_1, J_2, J'_0, J'_1, J'_2.

We can now give conditions for TEM modes being the lowest modes:

6C1 **Corollary 3.6.** *Let* Ω *by a circular cylinder of radius* R *and* $\Omega' = \Omega\setminus\Omega_{\mathsf{cd}}$, *with* Ω_{cd} *a coaxial cylinder of radius* r_0 *and the same length* ℓ.

(i) *In case of boundary conditions* (2.4b), *for any integer* $k\geq 1$ *such that*

$$\min\left\{\frac{z^{\mathsf{dir}}_{0,1}}{R}, \sqrt{\Big(\frac{z^{\mathsf{neu}}_{1,1}}{R}\Big)^2+\Big(\frac{\pi}{\ell}\Big)^2}\right\} > \frac{k\pi}{\ell} \quad \textit{i.e.} \quad k<\min\left\{0.766\frac{\ell}{R}, \sqrt{\Big(0.586\frac{\ell}{R}\Big)^2+1}\right\},$$

the following TEM mode in Ω' *corresponds to an eigenfrequency lower than those of* Ω:

TEMsin1 (3.14) $$\begin{cases} E_r = \frac{i}{r}\sin\left(\frac{k\pi}{\ell}z\right), \\ E_\theta = 0, \\ E_z = 0, \end{cases} \quad \textit{and} \quad \begin{cases} H_r = 0, \\ H_\theta = \frac{1}{r}\cos\left(\frac{k\pi}{\ell}z\right), \\ H_z = 0. \end{cases}$$

(ii) *In case of boundary conditions* (2.26a), *for any integer* $k\geq 1$ *such that*

$$\frac{z^{\mathsf{neu}}_{1,1}}{R} > \frac{k\pi}{\ell} \quad \textit{i.e.} \quad k<0.586\,\frac{\ell}{R},$$

the following TEM mode in Ω' corresponds to an eigenfrequency lower than those of Ω:

TEMsin2 (3.15)
$$\begin{cases} E_r = -\frac{i}{r}\cos\left(\frac{k\pi}{\ell}z\right), \\ E_\theta = 0, \\ E_z = 0, \end{cases} \quad \textit{and} \quad \begin{cases} H_r = 0, \\ H_\theta = \frac{1}{r}\sin\left(\frac{k\pi}{\ell}z\right), \\ H_z = 0. \end{cases}$$

(iii) *In case of boundary conditions* (2.26b)*, for any integer $k \geq 1$ such that*

$$\sqrt{\left(\frac{z^{\mathsf{neu}}_{1,1}}{R}\right)^2 + \left(\frac{\pi}{2\ell}\right)^2} > \left(k - \frac{1}{2}\right)\frac{\pi}{\ell} \quad \textit{i.e.} \quad k < \sqrt{\left(0.586\frac{\ell}{R}\right)^2 + \frac{1}{4}} + \frac{1}{2}\,,$$

the following TEM mode in Ω' corresponds to an eigenfrequency lower than those of Ω:

TEMsin3 (3.16)
$$\begin{cases} E_r = \frac{i}{r}\sin\left(k-\frac{1}{2}\right)\left(\frac{\pi}{\ell}z\right), \\ E_\theta = 0, \\ E_z = 0, \end{cases} \quad \textit{and} \quad \begin{cases} H_r = 0, \\ H_\theta = \frac{1}{r}\cos\left(k-\frac{1}{2}\right)\left(\frac{\pi}{\ell}z\right), \\ H_z = 0. \end{cases}$$

6R1 *Remark* 3.7. Let f be the frequency associated with ω, i.e. $\omega = 2\pi f$. Let c denote the speed of light. We have the relation $\omega = c\kappa$.

(i) In case of boundary conditions (2.4b) or (2.26a), the frequency ω associated with TEM modes is

TEMom (3.17)
$$\omega = \frac{k\pi c}{\ell}\,, \quad k = 1, 2, \ldots.$$

For the first TEM mode, we have $2\ell f = c$, which means that ℓ is the half-wave length.

(ii) In case of boundary conditions (2.26b), $4\ell f = c$, i.e., ℓ is the quarter-wave length of the first TEM mode.

6R2 *Remark* 3.8. *(i)* In accordance with lateral boundary conditions, all TE or TM eigenfrequencies have the form

3E80 (3.18)
$$\sqrt{\lambda^2 + \left(\frac{k\pi}{\ell}\right)^2} \quad \text{or} \quad \sqrt{\lambda^2 + \left(\frac{(k-\frac{1}{2})\pi}{\ell}\right)^2},$$

where λ spans the set of positive roots of special functions F_n. The standard case of the disk of radius R corresponds to $\lambda \mapsto J_n(\lambda R)$ or $\lambda \mapsto J_n'(\lambda R)$. For the case of G', annulus of radii r_0 and R, $F_n(\lambda)$ is a determinant:

3E81 (3.19)
$$F_n(\lambda) = J_n(\lambda r_0)\, Y_n(\lambda R) - Y_n(\lambda r_0)\, J_n(\lambda R) \quad \text{(Dirichlet case)}$$

with the Bessel function of the second kind Y_n. For the Neumann case, replace J_n and Y_n by their derivatives.

(ii) As a part of the discussion on artificial boundary conditions for our physical problem, we may think of imposing $\mathbf{H} \times \mathbf{n} = 0$ on $\partial G \times I$, instead of $\mathbf{H} \cdot \mathbf{n} = 0$. However, on $\partial G_{\mathsf{cd}} \times I$ the condition $\mathbf{H} \cdot \mathbf{n} = 0$ will still be imposed (perfect conductor approximation). For this new mixed problem, TEM modes do not exist. Only TE and TM modes appear, associated with eigenfrequencies of the form (3.18) for

3E82 (3.20) $$F_n(\lambda) = J_n(\lambda r_0)\, Y_n'(\lambda R) - Y_n(\lambda r_0)\, J_n'(\lambda R),$$

or with a permutation of derivatives.

4. Specifications for the incident magnetic field, the metallic conductor and the computational domain

S4 4.1. **Bird-cage coil.** As mentioned in the first section, the incident magnetic field $\boldsymbol{\mathcal{H}}_{\mathsf{inc}}$ is produced by a bird-cage coil (see an example in Fig. 1). Using an equivalent circuit analysis one gets the analytic formulas of the resonant frequencies of the coil. Then the magnetic field associated to each one is given by the Biot-Savart formula. In [3], an efficient algorithm for the computation of these fields has been developed. From numerical simulations it is seen that the magnetic field associated with the first resonant frequency of an N-leg coil is the only appropriate one for applications in MRI: This is the field used for our $\boldsymbol{\mathcal{H}}_{\mathsf{inc}}$. It is given by a discrete Fourier transform:

4E1 (4.1) $$\mathbf{H}_{\mathsf{inc}}(r,\theta,z) = \frac{\mu_0}{4\pi} \sum_{k=1}^{N} \mathbf{v}\left(r, \theta - \frac{2\pi k}{N}, z\right) \exp\left(\frac{2ik\pi}{N}\right),$$

where $\mathbf{v}$ is a function depending on the dimensions of the coil. We represent in Fig. 2 the modulus of the magnetic field $\mathbf{H}_{\mathsf{inc}}$ in the meridian domain Ω_{mer}. We remark that $\mathbf{H}_{\mathsf{inc}}$ is homogeneous in most of the coil. A theoretical and numerical analysis of this property and many more details can be found in [3]. In particular, it is verified that $\operatorname{div} \mathbf{H}_{\mathsf{inc}}$ is zero and, as a consequence of (4.1), the following property for $\mathbf{H}_{\mathsf{inc}}$ is proved: If developped in angular modes with respect to the axis of the coil, all coefficients are zero, except those of order n congruent to 1 modulo N.

Our specifications are the following: We use a 16 leg bird-cage coil with a diameter of 8.9 cm and a length of 12.8 cm. The width of the strip is 1 cm for the ring and 0.635 cm for the legs.

4.2. **Metallic wire.** The metallic conductor $\Omega_{\mathsf{cd}} = G_{\mathsf{cd}} \times I_{\mathsf{cd}}$ is a cylindrical wire of radius r_0 and length ℓ. Its axis is parallel to the bird-cage coil axis. Let ρ be the distance between the two axes. As mentioned in section 3, if ℓ is large enough, the smallest eigenfrequency belongs to a TEM mode. This is the reason why, from now on, we concentrate on the TEM modes. If $\rho = 0$, i.e. if the conductor and the coil are coaxial, we cannot expect that TEM modes around the conductor are excited, since TEM modes are axisymmetric and the angular mode of order 0 of the incident field is zero (see Fig. 4). Therefore in

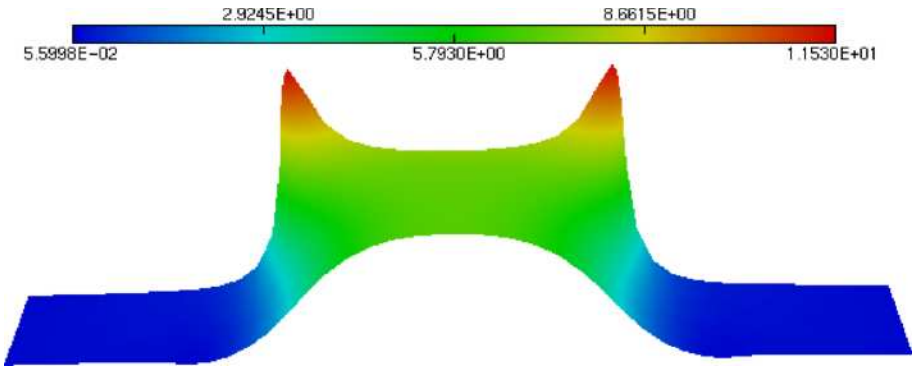

FIGURE 2. 3D view of the graph of $|\mathbf{H}_{\mathsf{inc}}|$ fighinc

the following we assume that $\rho \neq 0$, and we fix it to be 1 cm. In most of the numerical experiments, r_0 is equal to 1 cm and ℓ to 25.6 cm, see Fig. 3.

In all geometry graphs, the conductor is shown in red.

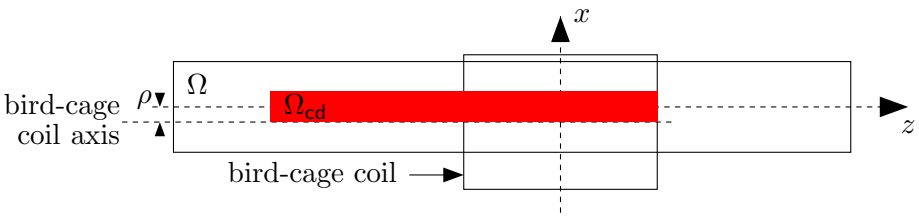

FIGURE 3. Projection on the xz-plane of the domains figomega

We represent in Fig. 4 $\|h^n_{inc}\|$ as a function of n for three values of ρ: $\rho = 0$ cm is indicated by circles, $\rho = 0.5$ cm by stars, and $\rho = 1$ cm by dots.

The conductivity σ of Ω_{cd} is set to 10^4 in most of our simulations. In a few experiments σ is set to a larger value, which will be specified.

4.3. **Computational domain and FEM discretization.** Our computational domain is $\Omega = G \times I$; it is a cylinder coaxial with Ω_{cd}. We assume that I contains I_{cd}, that the radius R of Ω is larger than r_0, but such that the projection G of Ω on the plane Π perpendicular to the axis is contained inside the projection of the coil on Π, namely R is set to 3 cm.

We mainly consider two different configurations for Ω:

(1) A full cartesian product form for the couple $(\Omega, \Omega_{\mathsf{cd}})$, i.e., $I = I_{\mathsf{cd}}$. This configuration is intended for validations of the finite element discretization. See in Fig. 5 the mesh of the meridian domain Ω_{mer} in the case when the radius of the conductor is 1 cm (the metallic conductor is in red). Each element is 6.4 cm by 1 cm.

(2) A configuration more relevant for the physical application: I has no common end with I_{cd}. The length of I is set to 44.8 cm. See in Fig. 6 the mesh in the case when

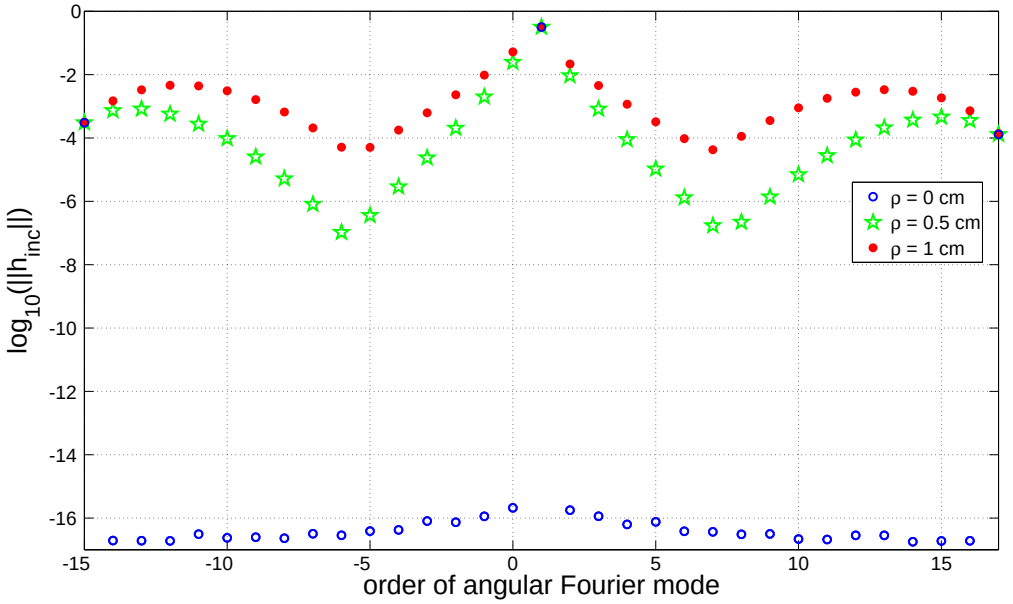

FIGURE 4. $\|h^n_{inc}\|$ versus n for three values of ρ figrho

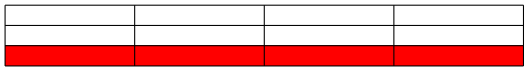

FIGURE 5. Mesh for full cylinder configurations (§5) figmeshtensor

the radius of the conductor is 1 cm. Rectangular elements have the same size as in Fig. 5.

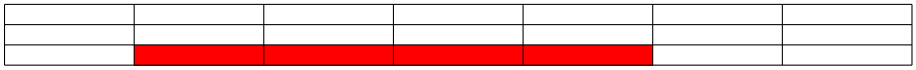

FIGURE 6. Mesh for "realistic" configurations (§6 & 7) figmesh

4.4. **Finite element discretizations.** On rectangular meshes in the meridian domain Ω_{mer} contained in the (r, z) plane, we use the Q10 elements (partial degree 10) available in the finite element library Melina (see [17]), and use the Galerkin discretization for the angular

mode 0 of the regularized Maxwell equations. The variational formulation is

4E7 (4.2) *Find* $\widetilde{\mathbf{H}} = (h_r, h_\theta, h_z) \in V$, *such that* $\forall \widetilde{\mathbf{H}}' = (h'_r, h'_\theta, h'_z) \in V$,

$$\int_{\Omega_{\mathsf{mer}}} \frac{1}{i\varepsilon\omega - \sigma} \Big(\partial_z h_\theta \, \partial_z h'_\theta + \tfrac{1}{r}\partial_r(r h_\theta) \, \tfrac{1}{r}\partial_r(r h'_\theta) + (\partial_r h_z - \partial_z h_r)\,(\partial_r h'_z - \partial_z h'_r) \Big) r \mathrm{d}r\mathrm{d}z$$
$$- \int_{\Omega_{\mathsf{mer}}} is\mu^2 \Big((\tfrac{1}{r}\partial_r(r h_r) + \partial_z h_z)(\tfrac{1}{r}\partial_r(r h'_r) + \partial_z h'_z) \Big) r \mathrm{d}r\mathrm{d}z$$
$$+ i\mu\omega \int_{\Omega_{\mathsf{mer}}} \widetilde{\mathbf{H}} \cdot \widetilde{\mathbf{H}}' \, r\mathrm{d}r\mathrm{d}z = -i\mu\omega \int_{\Omega_{\mathsf{mer}}} \widetilde{\mathbf{H}}^0_{\mathsf{inc}} \cdot \widetilde{\mathbf{H}}' \, r\mathrm{d}r\mathrm{d}z \, .$$

Here, $\mathbf{H}^0_{\mathsf{inc}}$ is the angular mode of order 0 of $\mathbf{H}_{\mathsf{inc}}$ *with respect to the axis of the conductor*.

The variational space V incorporates essential boundary conditions, in particular on the axis $r = 0$, where $h_r = h_\theta = 0$.

The computer code used to solve (4.2) is taken from [3], where it was created and validated. In particular, we can check that the solution is a divergence-free function and does not depend on the parameter s. With little modifications of this code, we could also solve the full 3D problem.

S5 5. FEM COMPUTATIONS IN FULL CARTESIAN PRODUCT CONFIGURATIONS

In this section, we consider a cartesian product structure: Ω and Ω_{cd} are two circular cylinders with the same length of 25.6 cm, meshed according to Fig. 5. Their common interval on the z axis is $I = (a, b)$. We investigate the influence of boundary conditions, and their accordance with theoretical results obtained in §2 and §3.

h.n 5.1. **Boundary condition $\mathbf{H} \cdot \mathbf{n} = 0$ on $\partial G \times I$.** We consider three cases associated with three combinations of boundary conditions:

- case 1: $\mathbf{H} \cdot \mathbf{n} = 0$ in $G \times \{a, b\}$,
- case 2: $\mathbf{H} \times \mathbf{n} = 0$ in $G \times \{a, b\}$,
- case 3: $\mathbf{H} \times \mathbf{n} = 0$ in $G \times \{a\}$ and $\mathbf{H} \cdot \mathbf{n} = 0$ in $G \times \{b\}$.

In the perfect conductor case (i.e., the limit as $\sigma \to \infty$), these three cases correspond to the framework theoretically investigated in §2 and 3. Extrapolating known results [16], we can expect a deviation from the limit by $\mathcal{O}(\sqrt{\sigma^{-1}})$, i.e., for $\sigma = 10^4$ by 1%.

We represent on Fig. 7 the variation of the $L^2(\Omega_{\mathsf{mer}}; r\mathrm{d}r)$-norm of the total angular component $h^{\mathsf{tot}}_\theta = h_\theta + (h_\theta)_{\mathsf{inc}}$ versus ω in each case: case 1 with circles, case 2 with stars and case 3 with dots. Integer multiples of 10^8 are sampled, from 1 to 250.

The expected values for resonant frequencies ω are the multiples of $\frac{\pi c}{\ell} \simeq 36.81 \times 10^8$ in cases 1 and 2, and half-multiples $(k - \frac{1}{2})$ for case 3. Our computations give the closest integer $\times 10^8$, for $k = 1, \ldots, 6$. We notice the difference in the amplitudes of even rank resonances for cases 1 and 2: This is due to quasi-orthogonality properties with adjoint

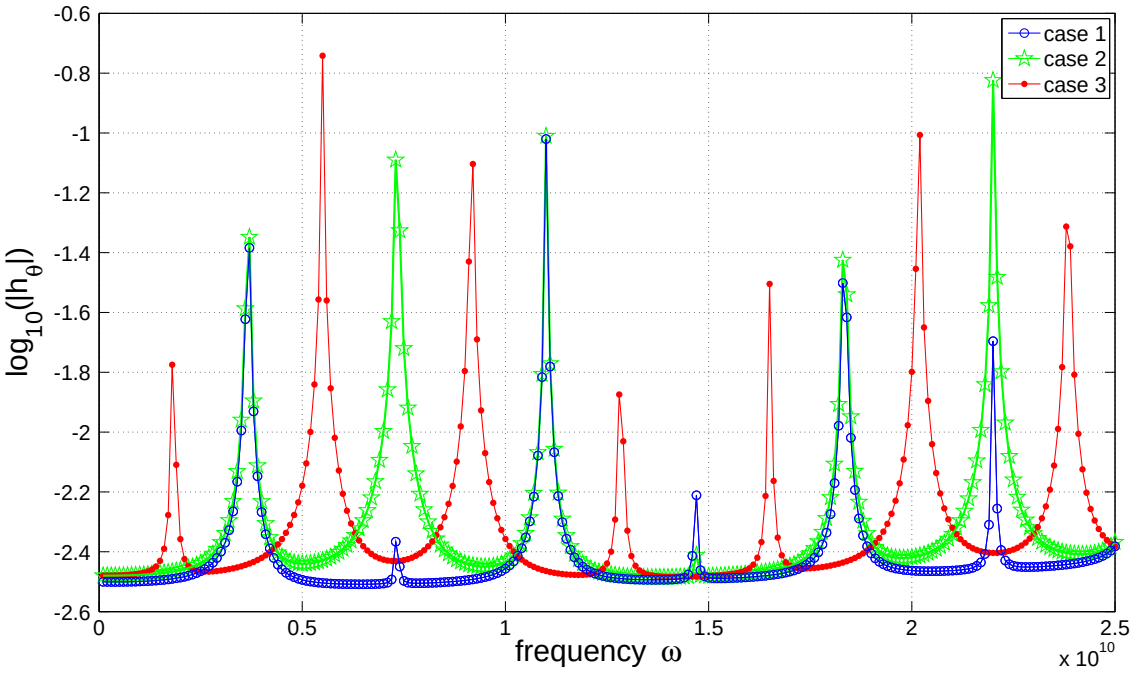

FIGURE 7. $\|h_\theta^{\text{tot}}\|$ versus ω for three combinations of lateral boundary conditions fig1s5

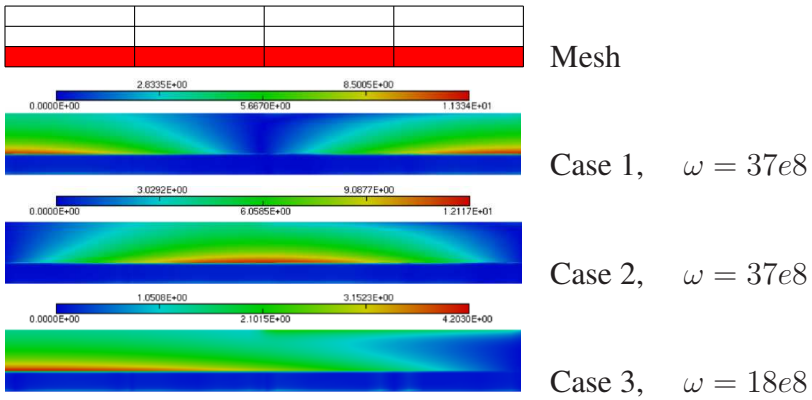

FIGURE 8. $|h_\theta^{\text{tot}}|$ associated with the first resonant frequency in Fig. 7 fig2as5

modes (the right hand side is supported in elements (1,3) and (1,4) of the mesh and has little variation in z).

We represent in Fig. 8 the absolute value $|h_\theta^{\text{tot}}|$ as function of (r, z) for the magnetic field associated with the first resonant frequency in each case.

hxn

5.2. **Boundary condition $\mathbf{H} \times \mathbf{n} = 0$ on $\partial G \times I$.** As mentioned in Remark 3.8, we can also consider the boundary condition $\mathbf{H} \times \mathbf{n} = 0$ on $\partial G \times I$ while keeping the same

boundary conditions on $G \times \{a\}$ and $G \times \{b\}$, but there will then be no TEM modes. We let the radius r_0 take three different values:

- case 1: $r_0 = 1$ cm,
- case 2: $r_0 = 1/4$ cm,
- case 3: $r_0 = 1/16$ cm.

The meshes are adapted to the varying inner radius, see below in §6.3.

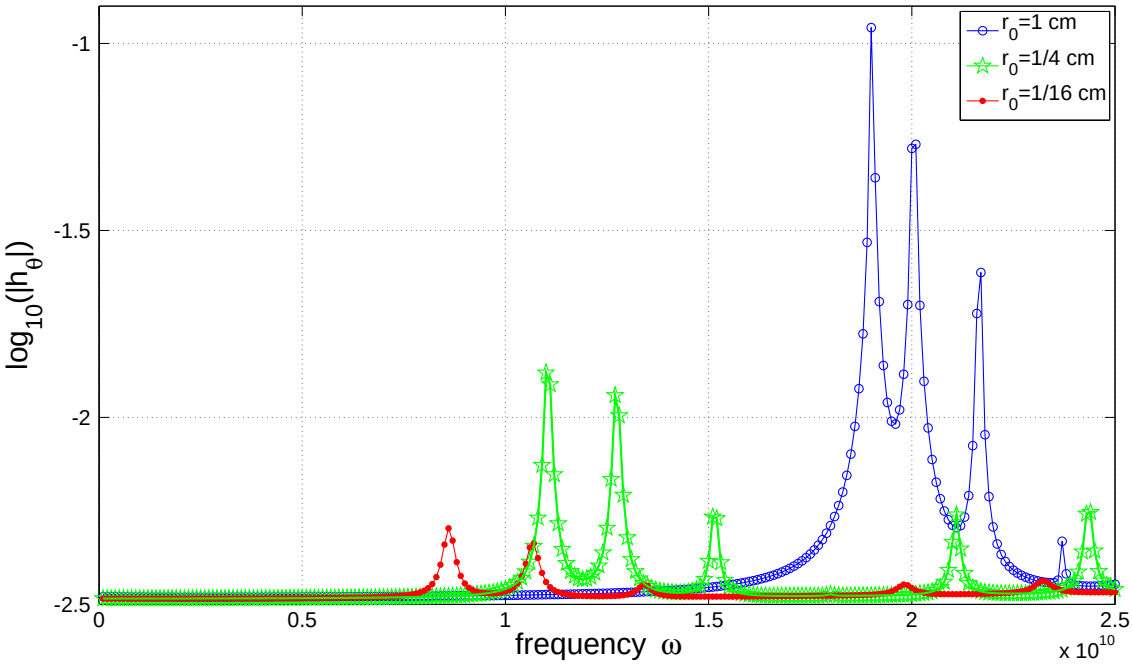

FIGURE 9. $\|h_\theta^{\text{tot}}\|$ versus ω for the boundary condition $\mathbf{H} \times \mathbf{n} = 0$ fig5s5

We represent in Fig. 9 the variation of the L^2-norm of h_θ^{tot} versus ω in each case: case 1 with circles, case 2 with stars and case 3 with dots. Computing the first root of the function F_0 (3.20), we find 62.560 for $r_0 = 0.01$, 34.957 for $r_0 = 0.0025$ and 26.481 for $r_0 = 0.000625$. Using formula (3.18), multiplying by $3e8$ and rounding to integers $\times 1e8$ we find exactly the same numbers as in Fig. 9.

In Fig. 10, we represent the absolute value of the magnetic field associated with the first resonant frequency when $r_0 = 1$ cm.

6. CONFIGURATIONS **B.** S6

We consider now the configuration depicted in Fig. 3, where the metallic conductor Ω_{cd} is completely surrounded by air. The domain Ω is not a cartesian product. Thus this case is not covered by the theory in §2 and §3, but this theory is expected to provide asymptotic models as the radius r_0 of the conductor tends to 0.

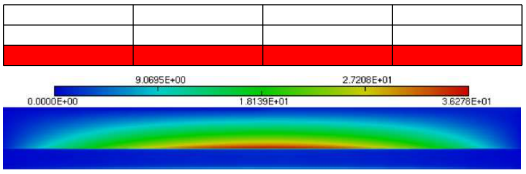

Mesh

$r_0 = 1$ cm, $\omega = 190e8$

FIGURE 10. $|h_\theta^{\text{tot}}|$ associated with the first resonant frequency

fig6s5

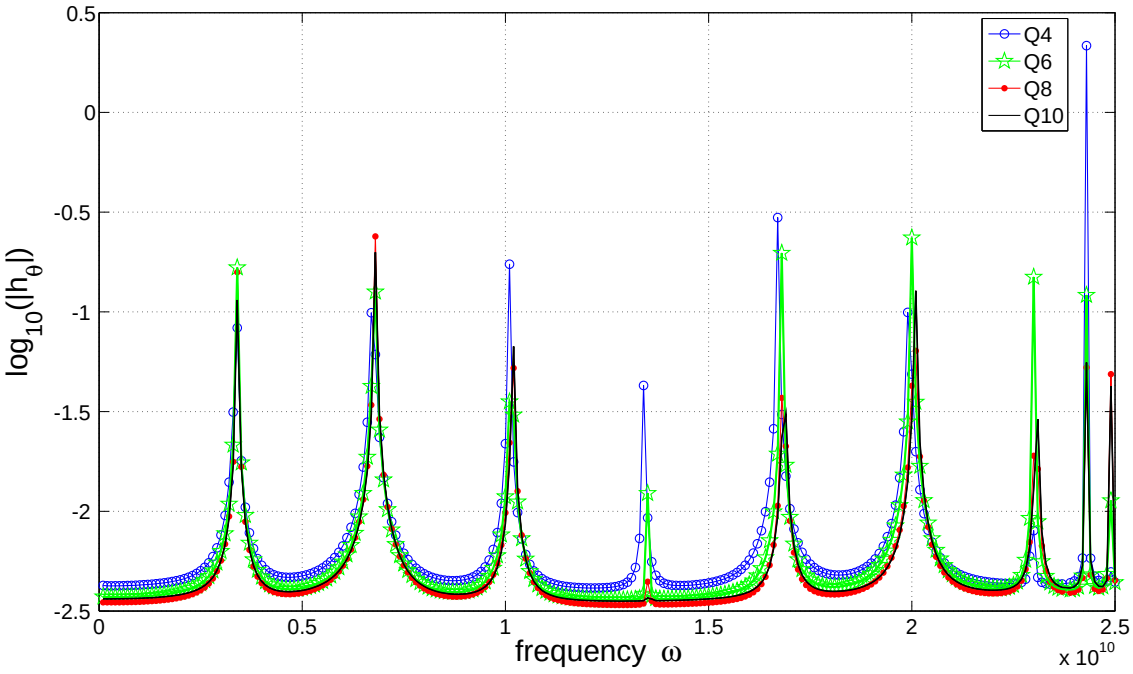

FIGURE 11. $\|h_\theta^{\text{tot}}\|$ versus ω for four interpolation degrees

fig7s5

6.1. **Interpolation degree.** We first check the convergence as the interpolation degree of the finite elements increases. We consider the boundary condition $\mathbf{H} \cdot \mathbf{n} = 0$ on $\partial\Omega$ and discretize problem (4.2) with four different degrees: Q4, Q6, Q8 and Q10. We represent in Fig. 11 the variation of the L^2-norm of h_θ^{tot} versus ω in each case: Q4 with circles, Q6 with stars, Q8 with points and Q10 with a solid line. The result shows that for the lowest resonances we already have a good precision with Q6 elements. A special case is the 4th resonance which we see disappear as the precision increases. As in the case observed above, this is due to the special geometry and the symmetry of the right hand side which makes it almost orthogonal to the corresponding eigenfunction of the adjoint problem. We deliberately chose a geometry with no global mirror symmetry (see Figure 6) in order to avoid more of such cancellations, but the fact that the bird-cage antenna covers just one-half of the length of the wire suffices for this cancellation of the 4th resonance.

6.2. **Varying boundary conditions.** As in the cartesian product case, the choice of boundary conditions on $\partial\Omega$ does have an important influence. We experiment with the following three combinations:

- case 1: $\mathbf{H}\cdot\mathbf{n}=0$ in $\partial\Omega$,
- case 2: $\mathbf{H}\cdot\mathbf{n}=0$ in $\partial G\times I$ and $\mathbf{H}\times\mathbf{n}=0$ in $G\times\{a,b\}$,
- case 3: $\mathbf{H}\times\mathbf{n}=0$ in $\partial\Omega$.

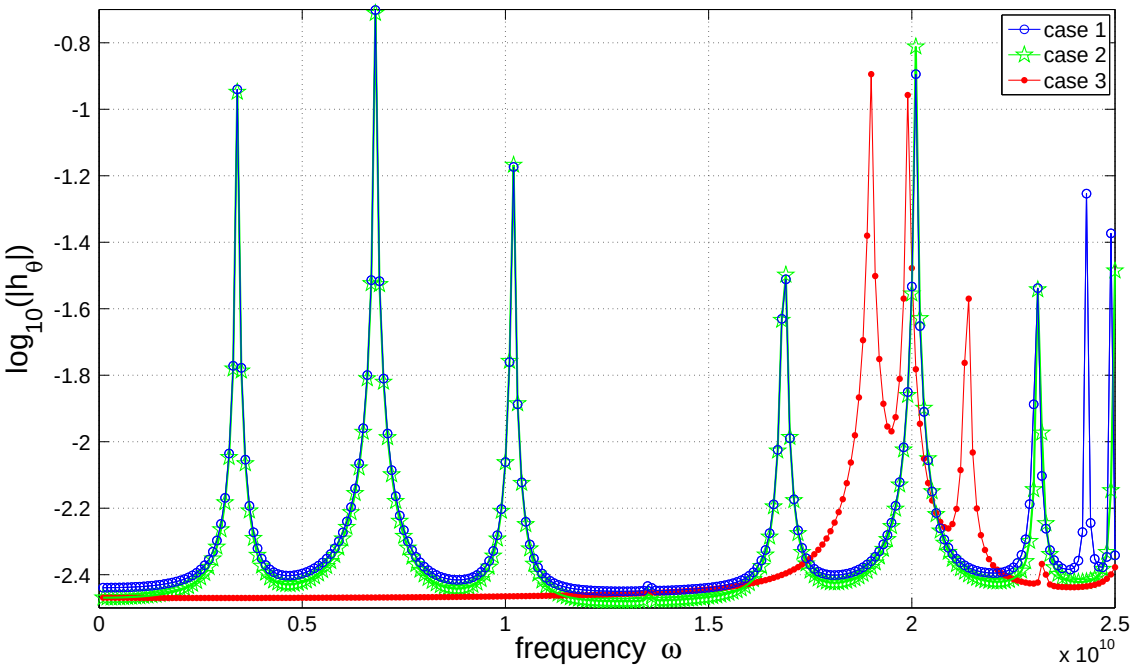

FIGURE 12. $\|h_\theta^{\mathrm{tot}}\|$ versus ω for three combinations of boundary conditions fig1s6

As we can see, there is almost no influence of the lateral boundary conditions on $G\times\{a,b\}$ (cases 1 and 2): The peaks coincide approximately with those of cases 1-2 in Fig. 7, and visibly correspond to TEM modes. We observe again the absence of the 4th resonance. The values of the resonant frequencies are very close to integer multiples of $c\pi/\ell_{\mathsf{cd}}\simeq 36.81\text{e}8$. The TEM structure is obvious in the "portraits" of the resonant modes, see Fig. 13. Beyond the 7th resonances we can glimpse the onset of the non-TEM modes.

Regardless of the lateral boundary conditions $G\times\{a,b\}$, the first resonant modes are close to the TEM modes in the domain $G\times I_{\mathsf{cd}}$ with lateral b.c. $\mathbf{H}\times\mathbf{n}=0$ (perfect insulator b.c.). In contrast, the boundary condition on the circular part $\partial G\times I$ has a strong influence: If set to $\mathbf{H}\times\mathbf{n}$, it kills the TEM modes, just as in the cartesian product case, see Fig. 9. Even in this case, the lateral boundary conditions do not play an important role: The resonant values in Fig. 9 (for $r_0=1$ cm) and 12 (case 3) are very close to each other.

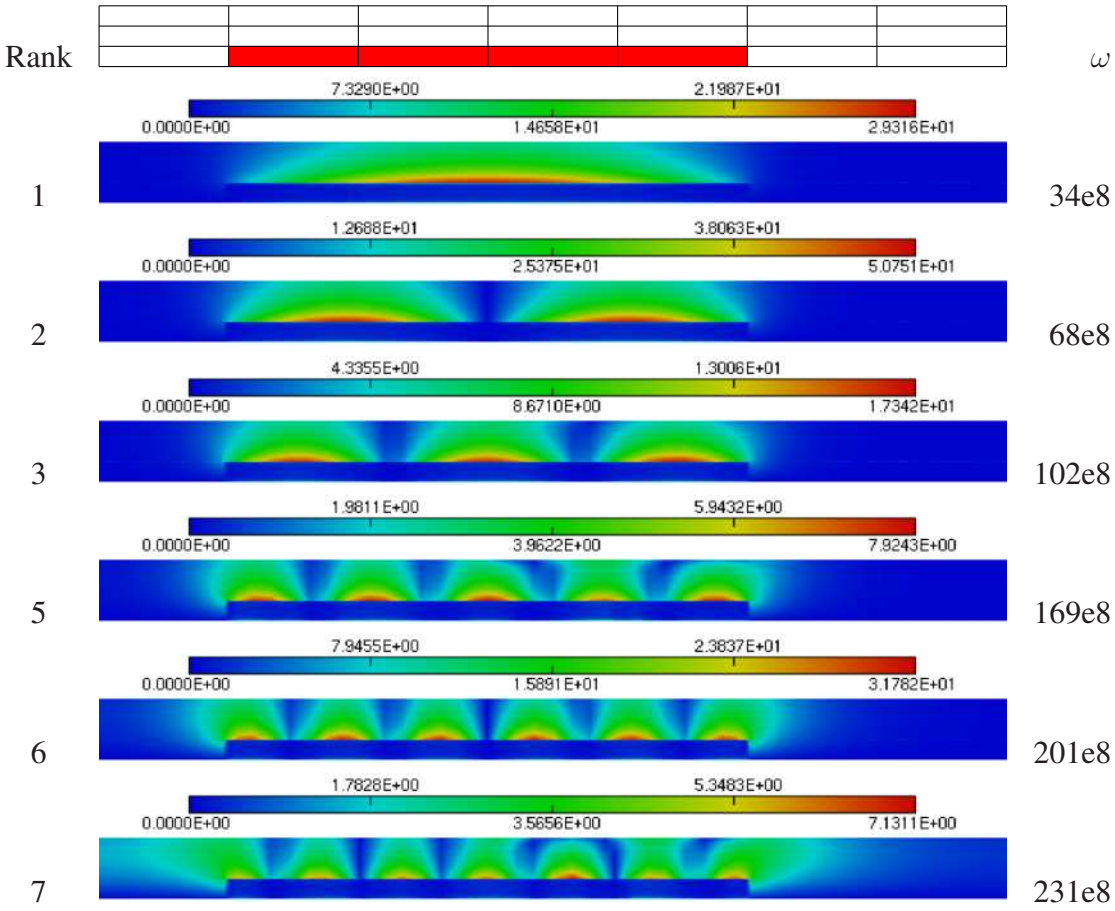

FIGURE 13. Resonant solutions with b.c. $\mathbf{H} \cdot \mathbf{n} = 0$ f1bs6

S6.3

6.3. **Varying the radius of the conductor.** As in §5.2, we now vary the radius r_0 of the conductor: 1 cm, $1/4$ cm and $1/16$ cm. For the numerical simulations we use two new tensor product meshes where the discretization in the z variable is the same as in Fig. 6 and is refined in the r variable: nodes at 0, $1/4$, 1, 2 and 3 cm when $r_0 = 1/4$ cm, and at 0, $1/16$, $1/4$, 1, 2 and 3 cm when $r_0 = 1/16$ cm.

In Figures 14 and 15, we see that the resonant frequencies vary only little, but the damping of the resonance as r_0 decreases is clearly visible. This is a consequence of the fact that the distance of penetration of the current inside the conductor (skin effect) is proportionally larger if σ is kept constant and the radius of the conductor decreases. We study the relation between σ and r_0 numerically in the next subsection.

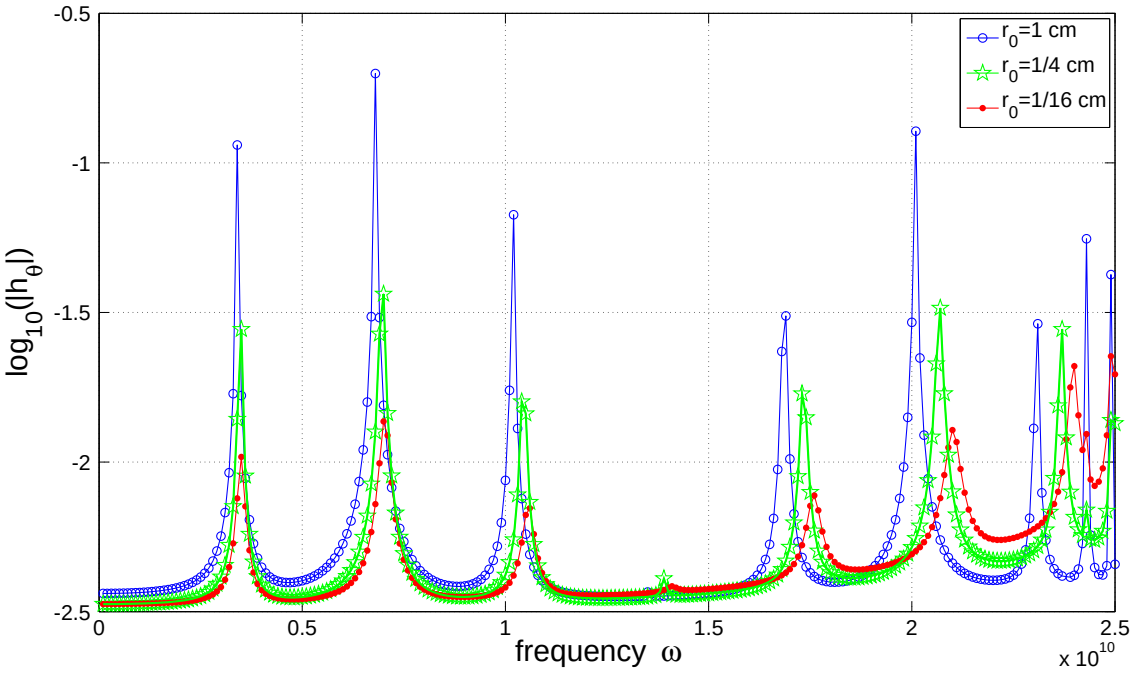

FIGURE 14. $\|h_\theta^{\text{tot}}\|$ versus ω for three conductor radii

fig2s6

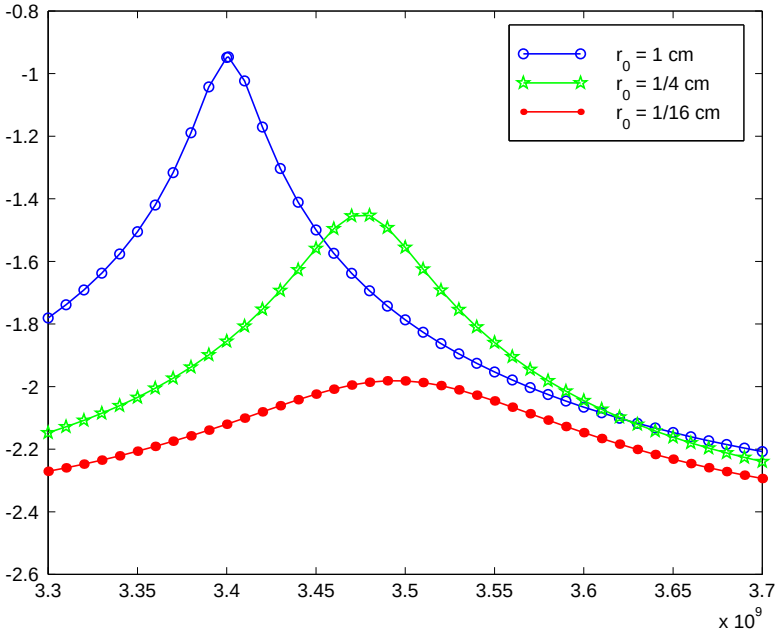

FIGURE 15. Zoom of Fig. 14 around ω =35e8

fig3s6

6.4. **Varying the conductivity as a function of the conductor radius.** From the theory of the skin effect, we know that the distance of penetration is proportional to $\sqrt{\sigma^{-1}}$. In Fig. 16, r_0 and σ are connected as follows:

- case 1: $r_0 = 1$ cm and σ =1e4,
- case 2: $r_0 = 1/4$ cm and σ =16e4,
- case 3: $r_0 = 1/16$ cm and σ =256e4,

so that $r_0\sqrt{\sigma}$ remains constant.

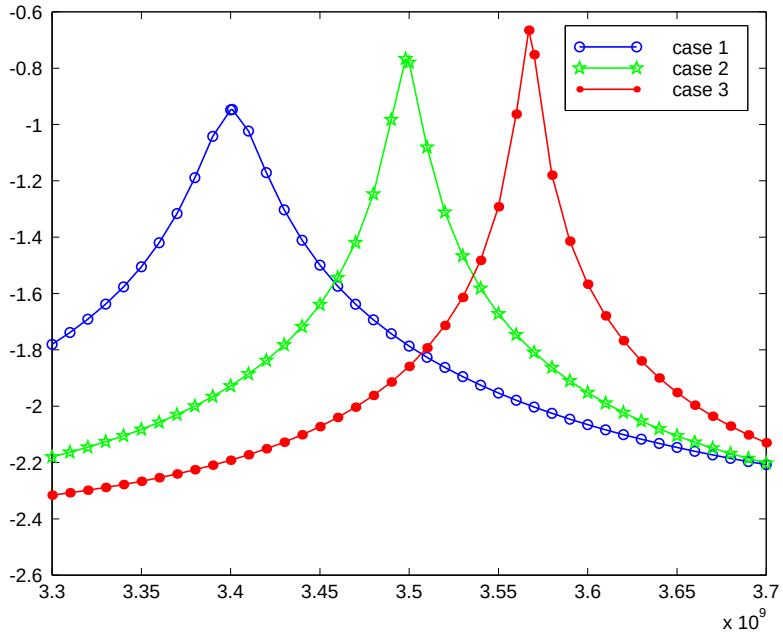

FIGURE 16. $\|h_\theta^{\text{tot}}\|$ versus ω for three conductor radii, with related σ fig5s6

We see that there is no more damping as r_0 decreases. We have evaluated the first resonance frequency ω_1 with four digit accuracy, for more values of r_0, see Table 2. We observe convergence to the perfect conductor situation in the case with connected σ, whereas there is no such convergence if σ is kept constant.

6.5. **Varying the length of the metallic conductor.** We have computed resonance frequencies for configurations like **B.**, with different values for the length ℓ of the metallic conductor. We keep the same 6.4 and 12.8 cm layers of air around the conductor. The conductor radius is 1 cm and the conductivity σ is 1e4. The results still agree with the law $c\pi/\ell$, as can be seen from Table 3.

7. CONFIGURATIONS **C.**

S7

Finally, we study configurations where the medium around the conductor may contain a part of dielectric or moderately conducting material (such as salted water).

r_0 in cm	1.0000	0.5000	0.2500	0.1250	0.0625
ω_1 with connected σ	34.01e8	34.50e8	34.98e8	35.37e8	35.67e8
Rel. deviation to $c\pi/\ell$	0.076	0.063	0.050	0.039	0.031
Convergence rate	-	0.27	0.34	0.35	0.33	-
ω_1 with constant σ =1e4	34.01e8	34.39e8	34.75e8	34.96e8	34.94e8
Rel. deviation to $c\pi/\ell$	0.076	0.066	0.056	0.050	0.051
Convergence rate	-	0.20	0.23	0.15	*	-

t2s6

TABLE 2. Variation of the first resonance frequency with r_0 and σ

Length ℓ in cm	25.6	32.0	38.4	44.8
Computed ω_1	34.0e8	27.6e8	23.2e8	20.0e8
$c\pi/\ell$	36.8e8	29.5e8	24.5e8	21.0e8
Rel. deviation to $c\pi/\ell$	0.076	0.063	0.055	0.050

t3s6

TABLE 3. The first resonant frequencies for different conductor lengths

7.1. **Metallic conductor surrounded by a moderately conducting material.** We first consider a homogeneous surrounding medium, namely the same configuration as in Fig. 3 with, instead of the air, $\varepsilon = 80\varepsilon_0$ in the medium surrounding the metallic conductor. We vary the electric conductivity in this medium: $\sigma = 0$, $\sigma = 0.01$, $\sigma = 0.1$, and $\sigma = 1$ and represent the response versus ω in Fig. 17.

We observe the opposite effect as when the conductivity of Ω_{cd} is increased. Note also that the corresponding TEM modes are associated with the eigenfrequencies $k\pi c'/\ell$, where c' is the speed of light inside the medium with relative permittivity 80. Thus $c' = c/\sqrt{80}$, and the TEM eigenfrequencies are the integer multiples of 4.116e8. The computed eigenfrequencies are 3.8e8, 7.6e8 and 11.3e8, instead of 4.1e8, 8.2e8 and 12.3e8.

7.2. **Metallic conductor surrounded by air and salt water.** In configuration in Fig. 3, we replace air with salted water in one, two or three columns of elements. On the mesh graphs, the region Ω_{swa} is in cyan (or light gray). We take $\varepsilon = 80\varepsilon_0$ and $\sigma = 4$ in the salt water.

In each of the three configurations, we show the first three resonant solutions in Fig. 19, 20 and 21.

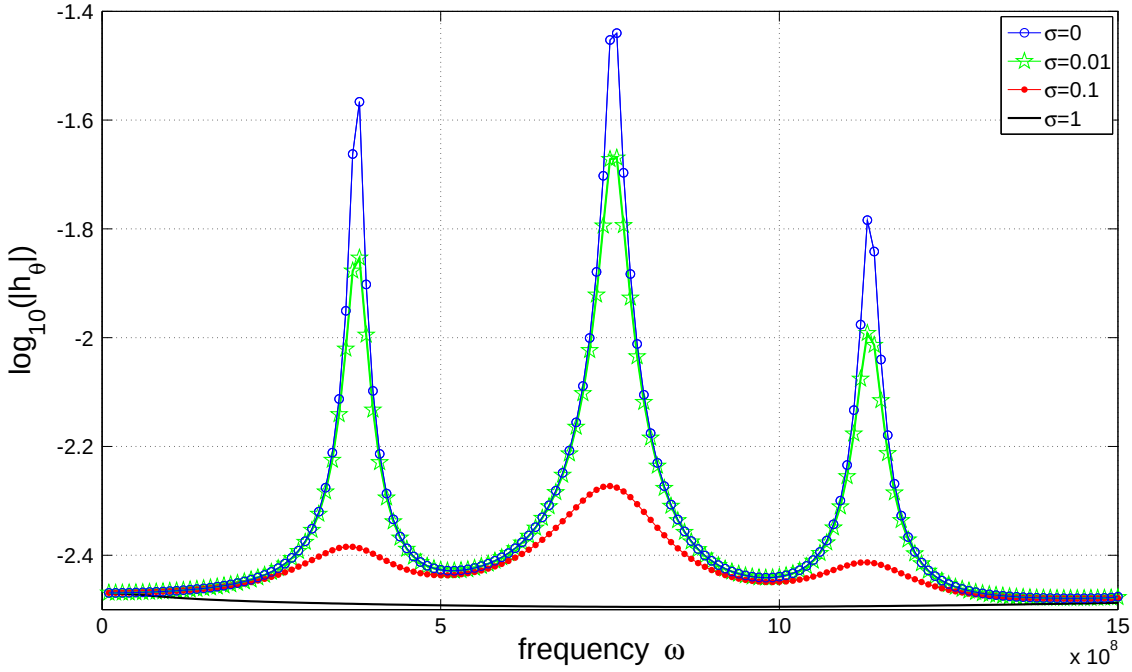

FIGURE 17. $\|h_\theta^{\text{tot}}\|$ versus ω for four different σ around the conductor

fig0bs7

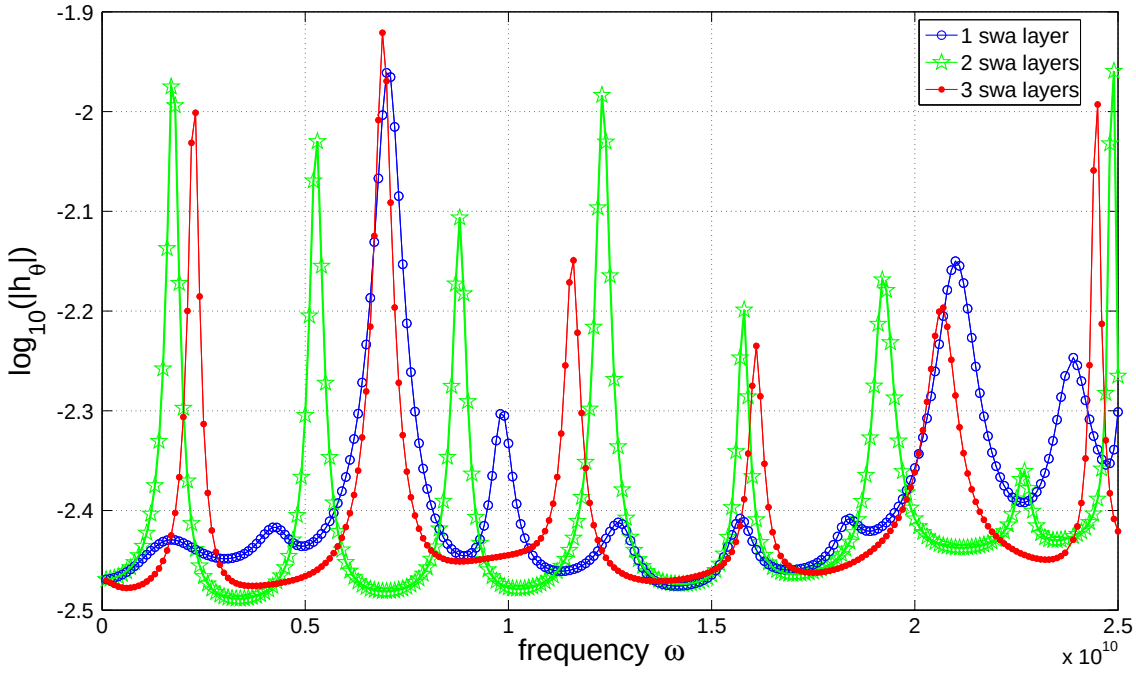

FIGURE 18. $\|h_\theta^{\text{tot}}\|$ versus ω with salt water layers

fig0s7

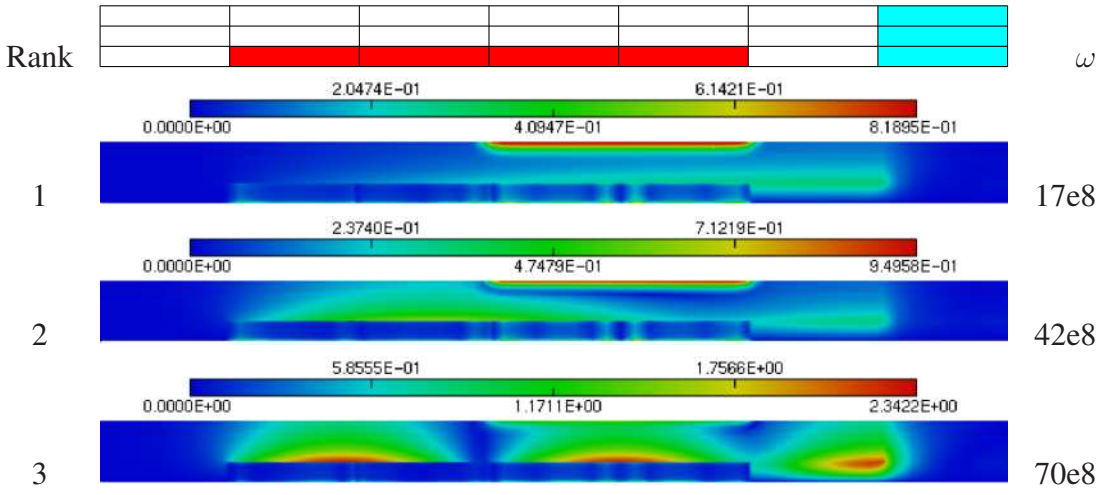

FIGURE 19. Resonant solutions with 1 salt water layer fig1as7

For the first two frequencies in Fig. 19, the resonance is so weak that one can clearly see the incident field in the plot (near the middle of the upper boundary). In all other field-strength plots with strong resonances, the incident field is hardly discernible.

Notice the similarities and differences of the rank 3 solution in Fig. 19 with the second resonant solution in Fig. 13. The approximate value of the second TEM eigenfrequency with perfectly insulating lateral b.c. is 73.6e8.

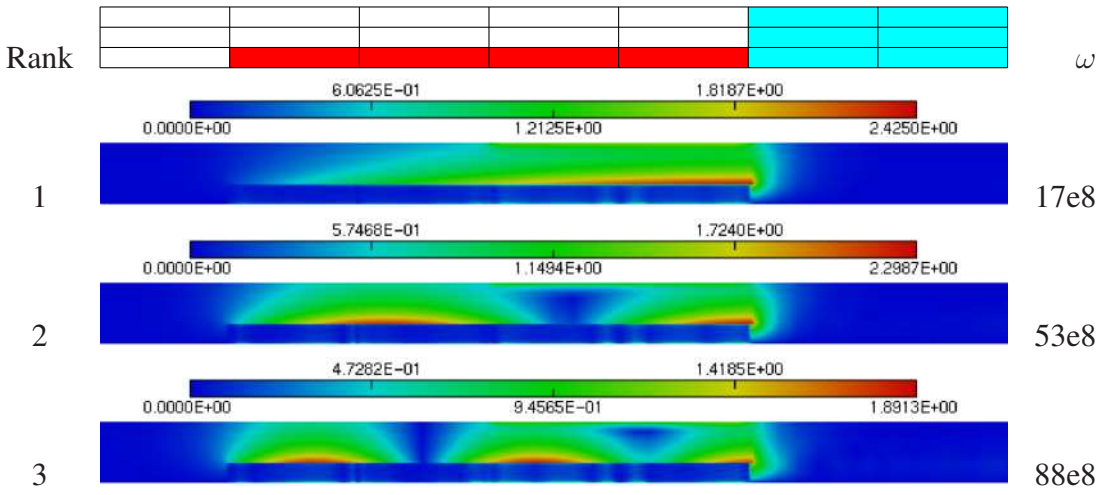

FIGURE 20. Resonant solutions with 2 salt water layers fig4as7

With two swa layers (Fig. 20), the metallic conductor has one of its ends in contact with water. The asymptotic model is then clearly the cartesian product configuration with

perfectly insulating b.c. in the right end and perfectly conducting b.c. in the left end. The TEM eigenfrequencies of this limit model are $c(k-\frac{1}{2})\pi/\ell$, namely approximately 18.4e8, 55.2e8, 92.0e8 for the first three ones.

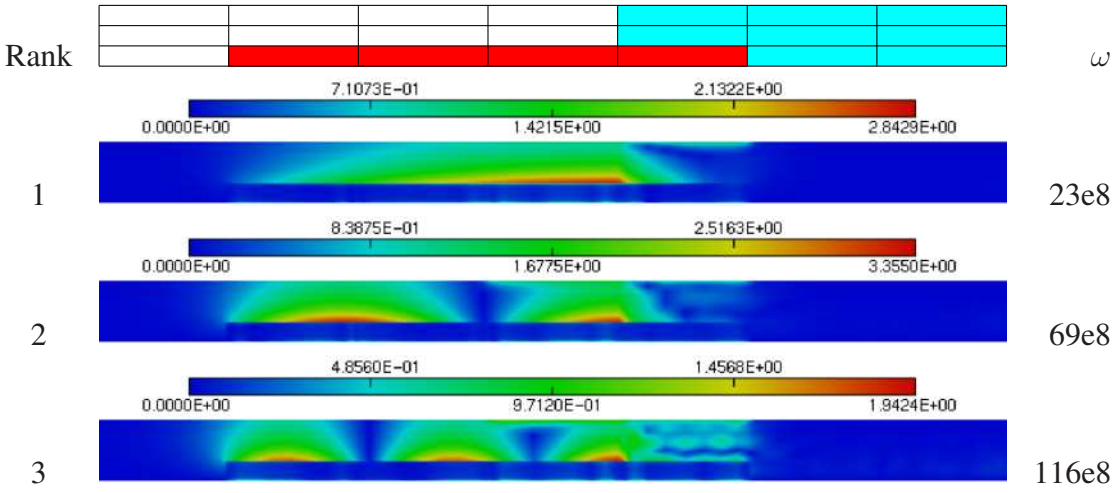

FIGURE 21. Resonant solutions with 3 salt water layers

fig7as7

With three swa layers (Fig. 21), one quarter of the metallic conductor lies in water. The asymptotic model is then the cartesian product configuration of length $\ell' = 3\ell/4$ with perfectly insulating b.c. in the right end and perfectly conducting b.c. in the left end. The TEM eigenfrequencies of this limit model are $c(k-\frac{1}{2})\pi/\ell'$, namely approximately 24.5e8, 73.6e8, 122.7e8 for the first three ones.

8. CONCLUSIONS

S8

In the numerical experiments in the previous sections, we studied the phenomenon that a conducting wire in an MRI device can act as a radiating antenna at certain resonance frequencies. Several general observations emerge quite clearly from the numerical results:

1. The strong variations of the field strength, in particular at the wire tips due to the singular geometry, but also at the surface of the wire and at the surface of the conducting liquid due to the skin effect, require a high-resolution discretization method. High order finite elements (of degree 8 or 10) on a rather simple structured grid are working well and give precise results.

2. The radiating-antenna modes can be described qualitatively, and in many cases also quantitatively with good accuracy, by the TEM modes of a greatly simplified mathematical model. The simplified mathematical model, a homogeneous material filling a circular cylinder with a coaxial cylindrical hole, has a small number of parameters that have to be chosen appropriately in order to get this agreement: Apart from the permittivity, mainly the length of the cylinder and the boundary conditions.

The length of the cylinder corresponds to the "effective" length of the wire. In the case of a wire surrounded by air, the effective length is a few percent longer than the physical length, due to the way how the field emerges from the wire tips. There is some minor influence from the form of the wire tips, although we have not presented this here. The maximal heat production corresponds to maximal strength of the electrical field which is attained also close to the wire tips, in general. Details of the behavior of the electric field could be obtained with high accuracy from a postprocessing of the computed magnetic field data which were presented here.

The diameter of the wire and its finite conductivity have an influence on the agreement between the numerical model and the simplified mathematical model, too: We observe convergence of the resonance frequencies of the former to the eigenfrequencies of the latter if the radius r_0 tends to 0 while the conductivity tends to infinity like r_0^{-2}.

In the case of a heterogeneous material consisting of air and a weakly conducting material (salt water), the effective length of the wire corresponds roughly to the length of the non-immersed part, if the wire is partially immersed. If the wire is entirely outside of the water, the situation is rather different. There can be cases where the space between the end of the wire and the surface of the water can contribute to the resonance and thus augment the effective length, by 50% in the case depicted in the third plot of Figure 19. The first resonances can be strongly damped in this case, too.

In the simplified mathematical model we always consider perfect conductor boundary conditions ($\mathbf{H} \cdot \mathbf{n} = 0$ and $\mathbf{E} \times \mathbf{n} = 0$) on the cylindrical surface corresponding to the wire, whereas the lateral boundary conditions are adapted to the different physical situations: In the case of a wire surrounded by air, the lateral boundary conditions to choose are perfect insulator conditions ($\mathbf{H} \times \mathbf{n} = 0$ and $\mathbf{E} \cdot \mathbf{n} = 0$). In the presence of salt water, the appropriate conditions corresponding to the surface of the liquid are the perfect conductor conditions.

3. The computational domain was chosen to be a circular cylinder coaxial to and radially centered around the wire with a radius smaller than the distance of the wire to the MRI bird-cage antenna. We showed results for different choices of boundary conditions on the artificial boundary of this domain. It turns out that if the computational domain is substantially longer than the wire, then the boundary conditions on the lateral parts of the boundary (bases of the cylinder) play almost no role. The boundary condition on the outer part of the boundary, which is also closest to the bird-cage antenna, are important, however. The radiating-antenna modes appear when perfect conductor conditions are chosen, and they are absent when perfect insulator conditions are chosen. This is also in agreement with the discussion of TEM modes for the simplified mathematical model.

4. The finite element library on which the numerical code was based allows easy adaptation of the model to other geometries and the treatment of various possible extensions: Testing of impedance conditions, for example, or full three–dimensional computations.

In the case of a hexahedral computational domain, one could again compare the numerical results with analytic separation-of-variables expressions for the eigenfrequencies and eigensolutions.

REFERENCES

ardiDaugeGirault98 [1] C. Amrouche, C. Bernardi, M. Dauge, and V. Girault. Vector potentials in three-dimensional non-smooth domains. *Math. Meth. Appl. Sci.*, 21:823–864, 1998.

ardiDaugeMaday99 [2] C. Bernardi, M. Dauge, and Y. Maday. *Spectral Methods for Axisymmetric Domains*, volume 3 of *Series in Applied Mathematics (Paris)*. Gauthier-Villars, Éditions Scientifiques et Médicales Elsevier, Paris, 1999.

PatriceThese [3] P. Boissoles. Problèmes mathématiques et numériques issus de l'imagerie par résonance magnétique nucléaire. Doctoral thesis, Université de Rennes 1, 2005.

BoisCaloz [4] P. Boissoles and G. Caloz. Accurate calculation of mutual inductance and magnetic fields in a birdcage coil. Preprint 06-07, Université de Rennes 1, 2006.

Chinellato [5] O. Chinellato, P. Arbenz, M. Streiff, and A. Witzig. Computation of optical modes in axisymmetric open cavity resonators. *Future Generation Computer Systems*, 21(8):1263–1274, 2005.

codaeig [6] M. Costabel and M. Dauge. Maxwell and Lamé eigenvalues on polyhedra. *Math. Methods Appl. Sci.*, 22:243–258, 1999.

CoDaDurham03 [7] M. Costabel and M. Dauge. Computation of resonance frequencies for Maxwell equations in non-smooth domains. In *Topics in Computational Wave Propagation*, volume 31 of *Lect. Notes Comput. Sci. Eng.*, pages 125–161. Springer, Berlin, 2003.

CourantHilbert53 [8] R. Courant and D. Hilbert. *Methods of Mathematical Physics. Vol. I.* Interscience Publishers, Inc., New York, N.Y., 1953.

Dempsey1 [9] M. F. Dempsey, B. Condon, and D. M. Hadley. Investigation of the factors responsible for burns during MRI. *J. Magn. Reson. Imaging*, 13:627–631, 2001.

HazardLenoir [10] C. Hazard and M. Lenoir. On the solution of time-harmonic scattering problems for Maxwell's equations. *SIAM J. Math. Anal.*, 27 (6):1597–1630, 1996.

HiptLedger [11] R. Hiptmair and P. D. Ledger. Computation of resonant modes for axisymmetric Maxwell cavities using hp-version edge finite elements. *Internat. J. Numer. Methods Engrg.*, 62(12):1652–1676, 2005.

Jones1 [12] S. Jones, W. Jaffe, and R. Alvi. Burns associated with electrocardiographic monitoring during magnetic resonance imaging. *Burns*, 22(5):420–421, 1996.

Konings1 [13] M. K. Konings, L. W. Bartels, H. F. Smits, and C. J. Bakker. Heating around intravascular guidewires by resonating RF waves. *J. Magn. Reson. Imaging*, 12:79–85, 2000.

Lewin1 [14] J. S. Lewin, A. Metzger, and W. R. Selman. Intraoperative magnetic resonance image guidance in neurosurgery. *J. Magn. Reson. Imaging*, 12:512–524, 2000.

Luechinger1 [15] R. Luechinger, F. Duru, R. Candinas, and P. Boesiger. Safety considerations for magnetic resonance imaging of pacemaker and ICD patients. *Herzschr Elektrophys*, 15:73–81, 2004.

MacCamyStephan [16] R. C. MacCamy and E. Stephan. A skin effect approximation for eddy current problems. *Arch. Rational Mech. Anal.*, 90(1):87–98, 1985.

melina [17] D. Martin. Mélina. Online documentation: `http://perso.univ-rennes1.fr/daniel.martin/melina`.

PardoDTVT [18] D. Pardo, L. Demkowicz, C. Torres-Verdín, and L. Tabarovsky. A goal-oriented hp-adaptive finite element method with electromagnetic applications. I. Electrostatics. *Internat. J. Numer. Methods Engrg.*, 65(8):1269–1309, 2006.

Pictet1 [19] J. Pictet, R. Meuli, S. Wicky, and J. J. van der Klink. Radiofrequency heating around resonant lengths of wire in MRI. *Physics in Medecine and Biology*, 47:2973–2985, 2002.

Yeung7 [20] B. Qiu, C. J. Yeung, X. Du, E. Atalar, and X. Yang. Development of an intravascular heating source using an MR imaging guidewire. *J. Magn. Reson. Imaging*, 16:716–720, 2002.